

**Exact Scattering from a Parabolic Cylinder Coated in an Isorefractive
Sheath**

BY

PATRICK MARTIN

B.S., University of Wisconsin - Madison, 2010

M.S., University of Illinois at Chicago, 2016

THESIS

Submitted as partial fulfillment of the requirements
for the degree of Master of Science in Electrical and Computer Engineering
in the Graduate College of the
University of Illinois at Chicago, 2019

Chicago, Illinois

Defense Committee:

Danilo Erricolo, Chair and Advisor

Piergiorgio L.E. Uslenghi

Pai-Yen Chen

Copyright by
PATRICK MARTIN
2019

To my wife, Molly.

ACKNOWLEDGMENT

I would first like to thank my advisor, Prof. Danilo Erricolo, for his assistance and input on this thesis. Without his guidance and expertise, this paper would not be possible.

I would like to thank my entire thesis committee, Prof. Danilo Erricolo, Prof. Piergiorgio L. E. Uslenghi and Prof. Pai-Yen Chen, for their time and energy in reviewing this thesis, and their support and assistance throughout the process.

I would next like to thank the University of Illinois at Chicago, specifically the departments of Electrical and Computer Engineering, and Physics, for not only allowing me the opportunity to study at the university with wonderful professors and students, but also for the financial support which made it all possible.

I would like to thank my current employer, Northrop Grumman, for financially supporting the completion my studies. I would also like to thank many of the people I work with at Northrop Grumman for their flexibility in working with me while completing this thesis, including Mike Davis, Michael Moore, Heather Kang, Curtis Harkrider, Ben Wallace, Jim Atwood, Ron Jones, Mike Kernal, James Kless, Gerardo De La Torre, Jeremy Feldstein and Mike Johnson.

I would like to thank my parents, Brian and Suzanne, for their love and support throughout the years. They always nurtured my curiosity, despite the dangerous results of my early experiments.

ACKNOWLEDGMENT (Continued)

I would like to thank my siblings, Anne Rose and Michael, for their encouragement. Our perpetual sibling rivalry forces me to always improve myself, and I believe this thesis gives me a momentary lead.

Finally, I would like to thank my wife, Molly, for her love, support, advice and friendship. She is the only one who can bring me back to earth when I float off into space.

PJM

TABLE OF CONTENTS

<u>CHAPTER</u>	<u>PAGE</u>
1 INTRODUCTION	1
1.1 The Isorefractive Condition	2
1.2 Geometry	4
1.2.1 Cartesian to Parabolic Cylinder Coordinates	4
1.2.2 Geometry of the Problem	8
1.2.3 Circular Cylinder to Parabolic Cylinder Coordinates	10
1.3 Calculus and the Parabolic Cylinder Functions	11
1.4 Boundary Value Problems Background	13
2 ANALYTIC SOLUTIONS	15
2.1 Plane Wave Source - Electric Polarization	15
2.2 Simple PEC Scattering Limit	22
2.3 Plane Wave Source - Magnetic Polarization	24
3 NUMERICAL CALCULATIONS - BACKGROUND PROBLEMS	30
3.1 Introduction	30
3.2 PEC Scattering	31
3.3 Isorefractive Scattering	33
4 NUMERICAL CALCULATIONS - ISOREFRACTIVE SHEATH	36
4.1 Introduction	36
4.2 Near-Field Simulation	36
4.3 Far-Field Asymptotic Derivation	40
4.4 Computational Considerations	44
4.5 Convergence of the Infinite Sum	50
4.6 The Scattered Field	62
4.7 Software	76
5 CONCLUDING REMARKS	77
APPENDIX	79
CITED LITERATURE	101
VITA	106

LIST OF TABLES

<u>TABLE</u>		<u>PAGE</u>
I	VALUES USED FOR CALCULATING FIELDS	51

LIST OF FIGURES

<u>FIGURE</u>		<u>PAGE</u>
1	Parabolic cylinder geometry	5
2	Geometry setup of the scattering problem	9
3	Near-field electric field for a PEC parabolic cylinder	32
4	Boundary value condition for a PEC parabolic cylinder	33
5	Near-field electric field for an isorefractive parabolic cylinder	34
6	Boundary value condition for an isorefractive parabolic cylinder	35
7	Near-field electric field for an isorefractive sheath of width $\frac{7\lambda}{4}$	37
8	Boundary value condition for an isorefractive sheath of width $\frac{7\lambda}{4}$	38
9	Near-field electric field for an isorefractive sheath of width λ	39
10	Boundary value condition for an isorefractive sheath of width λ	39
11	$F_n(\phi)$ vs. ϕ	45
12	$ p_n(\phi_0) $ vs. n	47
13	a_n vs. n	48
14	Product of a_n and $p_n(\phi_0)$ vs. n	49
15	Far-field scattering, $ \Psi_s(\phi) $, $\phi_0 = \pi$	63
16	Far-field scattering phase angle of $\Psi_s(\phi)$, $\phi_0 = \pi$	64
17	Far-field scattering, $ \Psi_s(\phi) $, $\phi_0 = \frac{17\pi}{18}$	66
18	Far-field scattering phase angle of $\Psi_s(\phi)$, $\phi_0 = \frac{17\pi}{18}$	67
19	Far-field scattering, $ \Psi_s(\phi) $, $\phi_0 = \frac{3\pi}{4}$	69

LIST OF FIGURES (Continued)

<u>FIGURE</u>		<u>PAGE</u>
20	Far-field scattering phase angle of $\Psi_s(\phi)$, $\phi_0 = \frac{3\pi}{4}$	70
21	Far-field scattering, $ \Psi_s(\phi) $, $\phi_0 = \frac{5\pi}{4}$	71
22	Far-field scattering phase angle of $\Psi_s(\phi)$, $\phi_0 = \frac{5\pi}{4}$	72
23	Far-field scattering, $ \Psi_s(\phi) $, $\phi_0 = \frac{11\pi}{18}$	74
24	Far-field scattering phase angle of $\Psi_s(\phi)$, $\phi_0 = \frac{11\pi}{18}$	75

LIST OF ABBREVIATIONS

PCF	Parabolic Cylindrical Wave Function
PEC	Perfect Electrically Conducting

SUMMARY

The problem of an electromagnetic plane wave scattering off a perfect electrically conducting parabolic cylinder embedded in a confocal parabolic cylinder made of a material isorefractive to the surrounding space is solved and analyzed. The parabolic cylinder geometry is introduced, and a number of mathematical and physical relations required for the evaluation of the problem are discussed. A set of exact, analytic solutions of the scattering problem are derived. Utilizing these solutions, the numerical calculation of the scattered field is analyzed for realistic input parameters and asymptotic limits. Plots of the scattered wave in the far field are presented and discussed for different incident angles. In the process of generating results for the full isorefractive sheath problem, the solutions to simpler problems of the scattering from parabolic cylinders of different materials are discussed, and the near-field behaviors are plotted.

This paper reveals a new, exact canonical solution to an electromagnetic scattering problem, one which can be used in benchmarking modeling software. It also presents an in-depth discussion of the convergent properties of the infinite sums which make up the expression of the scattered field, and provides a road map which can be followed in evaluating similar problems.

The plots of the scattered fields prove to be interesting in their own right, but only begin to scratch the surface of the problem space. Thus, an interesting problem, which is but one of a rich field of study, is solved.

CHAPTER 1

INTRODUCTION

Electromagnetic scattering is a fascinating subject. It affects our everyday lives, yet understanding scattering behavior requires knowledge of math, physics and electrical engineering. One can conceive of any number of interesting scattering geometries, yet only certain setups lend themselves to tractable solutions. The problem of the scattering of a plane wave by a metallic, Perfect Electrically Conducting (PEC) parabolic cylinder coated with a confocal isorefractive material will be our subject matter in this thesis. It requires a geometry that allows for the analysis of interesting shapes, i.e. the parabolic cylinder, but that is simple enough to work in comfortably.

A number of scattering problems have been solved in this geometry; the general problem of a plane wave scattering from a PEC parabolic cylinder has been solved in (1), the isorefractive parabolic cylinder was solved in (2), and the PEC cylinder coated in dielectric material has been solved in (3), however the geometry of a PEC coated in an isorefractive material has not been undertaken until now. (3) focused instead on numerical approximations, such as the method of moments, which allow for a general, but inexact, solution. The work in (4) concentrated on the case of a PEC spheroid coated in an isorefractive material, and we will take a similar approach, along with (2) and (5), to solve this problem.

After deriving the analytic solution for this problem, we will dive into investigating the numerical behavior of our solutions, especially as we try to find finite solutions. The rigorous

analysis we perform in 4.4 and 4.5 is novel to this problem setup and has not been tackled before. After showing that our methods and calculations will not lead to infinite or unphysical behavior, we will present the results of some interesting scattering setups. The only way that we can venture to take these steps is through the application of the isorefractive condition.

1.1 The Isorefractive Condition

Uslenghi coined the term *isorefractive* (2), which refers to two materials with the same index of refraction, but which may have different intrinsic impedances. Consider a material with permittivity $\epsilon_1 = \epsilon_0 \epsilon_{r1}$, where ϵ_0 is the vacuum permittivity and ϵ_{r1} is the relative permittivity. The material permeability is $\mu_1 = \mu_0 \mu_{r1}$, where similarly μ_0 is the vacuum permeability and μ_{r1} is the relative permeability. The index of refraction n_1 of the material is given by

$$n_1 = \sqrt{\epsilon_1 \mu_1} \quad (1.1)$$

and a wave traveling through this medium will have wavenumber

$$k_1 = \omega \sqrt{\epsilon_1 \mu_1} = \underbrace{\omega \sqrt{\epsilon_0 \mu_0}}_{k_0 \text{ vacuum}} \underbrace{\sqrt{\epsilon_{r1} \mu_{r1}}}_{n_1} \quad (1.2)$$

where ω is the angular frequency of the wave in the material. The material has intrinsic impedance

$$Z_1 = \sqrt{\frac{\mu_1}{\epsilon_1}} \quad (1.3)$$

and we will make use of the variable Y throughout this paper as the inverse impedance

$$Y_i = Z_i^{-1} = \sqrt{\frac{\epsilon_i}{\mu_i}}. \quad (1.4)$$

Two materials satisfy the isorefractive condition if $n_1 = n_2$, or more importantly for our needs,

$$\boxed{k_1 = k_2} \quad (1.5)$$

but it is not necessary that they share the same intrinsic impedance, i.e. $Z_1 \neq Z_2$. Many dielectric scattering boundary value problems have been solved through application of the isorefractive condition (6) (7) (8) (9) (10) (11) (12) (13) (14) (15) (16) (17) (18) (19) (20) (5) (21) (22) (23) (2) (24) (25) (26) (27) (28) (29) (30) (31) (32) (4) (33) (34) (35). The isorefractive condition becomes exceptionally useful when solving the system of equations that define the scattering problem. Without the isorefractive condition, one is forced to resort to approximation techniques such as the method of moments to solve the system of equations (3).

1.2 Geometry

1.2.1 Cartesian to Parabolic Cylinder Coordinates

We start by defining the problem space in parabolic-cylinder coordinates, η, ξ, z which relate to the Cartesian x, y, z by

$$x = \frac{1}{2}(\xi^2 - \eta^2) \quad (1.6a)$$

$$y = \xi\eta \quad (1.6b)$$

$$z = z \quad (1.6c)$$

where $\eta \geq 0$, $-\infty < \xi < \infty$, $-\infty < z < \infty$. Here we have used the convention of (1). The unit normal vectors, $\hat{\eta}$, $\hat{\xi}$ and \hat{z} are orthonormal to each other. The surface $z = \text{constant}$ defines a plane parallel to the typical Cartesian xy plane. The surface $\eta = \text{constant}$ defines a parabolic cylinder, i.e. a sheet which follows that path of a parabola about a common focus at the origin, and which extends to $\pm\infty$ in the z direction, and which opens along the positive x direction. Similarly, the surface $\xi = \pm\text{constant}$ defines a second parabolic cylinder with its focus located at the origin, but which opens in the negative x direction. This geometry is shown in Figure 1. Note here that we have chosen the \hat{z} direction to be *into* the page, i.e. in the Cartesian $-z$ direction, to agree with the right-hand rule as it applies to our convention of listing η as the first input argument to a function.

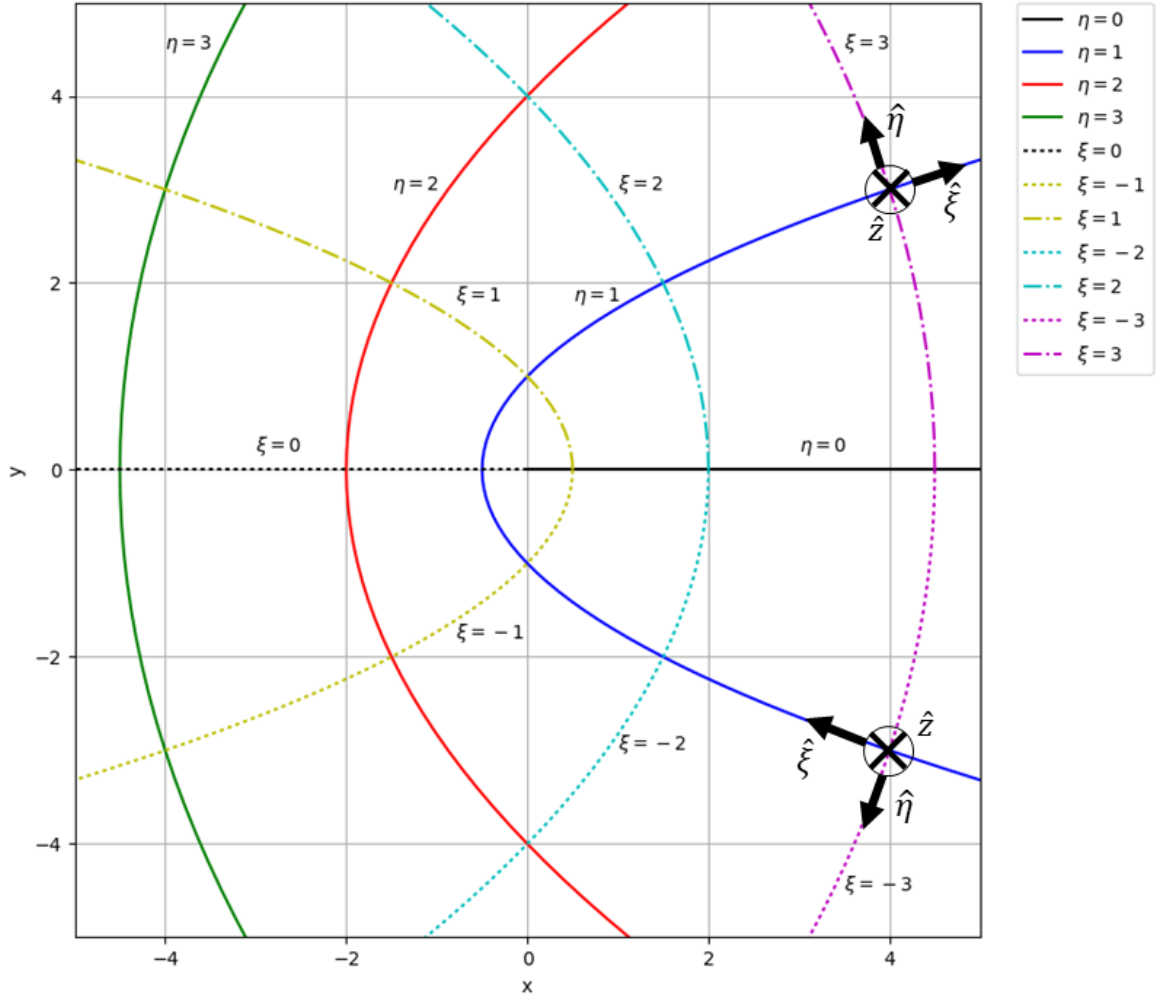


Figure 1: Parabolic cylinder geometry

It will be instructive to explore this geometry in a bit more depth. Consider Equation 1.6b, $y = \xi\eta$. If we set $\xi = 0$, then $y = 0$, and thus $x = -\frac{\eta^2}{2}$, which corresponds to the negative

x -axis, inclusive of the origin. Similarly, setting $\eta = 0$ also results in $y = 0$, but $x = \frac{\xi^2}{2}$, which corresponds to the positive x -axis, also inclusive of the origin.

We mentioned that the surface $\eta=\text{constant}$ is a parabolic cylinder, now if we rearrange Equation 1.6b as $\eta = \frac{y}{\xi}$, we find that Equation 1.6a can be expressed as

$$x = \frac{1}{2}(\xi^2 - \frac{y^2}{\xi^2}) \quad (1.7)$$

$$x = -\frac{y^2}{2\xi^2} + \frac{\xi^2}{2} \quad (1.8)$$

Recall from geometry class that a parabola takes the form

$$x = ay^2 + by + c \quad (1.9)$$

which for our setup corresponds to

$$a = -\frac{1}{2\xi^2}, \quad b = 0, \quad c = \frac{\xi^2}{2}. \quad (1.10)$$

Now the focal point F of this parabola can be calculated by

$$F = \left(\frac{4ac - b^2 + 1}{4a}, \frac{-b}{2a} \right) \quad (1.11)$$

and making these substitutions we find

$$F = \left(\frac{-4 \frac{1}{2\xi^2} \frac{\xi^2}{2} + 1}{-4 \frac{1}{2\xi^2}}, \frac{0}{-2 \frac{1}{2\xi^2}} \right) = (0, 0) \quad (1.12)$$

Thus we see that for any constant $\pm\xi$, the resulting parabola will have its focus at the origin, i.e. the parabolic surfaces are confocal. A similar approach with constant η instead of ξ will show the same relation.

Let us consider a few relations which may be helpful when working in this coordinate system. A simple relation to consider is the point on the x-axis at which the parabolic cylinder at $\eta = \eta_0$ crosses. This parabolic cylinder will always cross the x-axis at $x \leq 0$. Along the x-axis, $\xi = 0$, and so we can calculate the x intercept of a parabolic surface by

$$\eta_0^2 = -2x. \quad (1.13)$$

Any point along the negative x-axis will have coordinates $\xi = 0, \eta^2 = -2x$. Further, to calculate any arbitrary η and ξ from x and y , we use the relations

$$\eta^2 = \frac{y^2}{x + \sqrt{x^2 + y^2}} \quad (1.14)$$

and

$$\xi^2 = x + \sqrt{x^2 + y^2} \quad (1.15)$$

Since this calculation of ξ will always yield $\xi \geq 0$, we must set

$$\xi = -\sqrt{x + \sqrt{x^2 + y^2}} \quad (1.16)$$

if $y < 0$ and

$$\xi = \sqrt{x + \sqrt{x^2 + y^2}} \quad (1.17)$$

if $y > 0$.

1.2.2 Geometry of the Problem

In the layout of our problem, we have a PEC parabolic cylinder with its surface defined by $\eta = \eta_1$. The parabolic cylinder is encased in a sheath of penetrable, lossless dielectric material with an outer boundary defined on the curve $\eta = \eta_2$. The surrounding space is isorefractive to this boundary sheath, as seen in Figure 2. It may be helpful to point out that a field tangent to one of these parabolic cylinder surfaces will have components in the $\hat{\xi}$ and \hat{z} directions, and a field normal to this surface has components in the $\hat{\eta}$ direction.

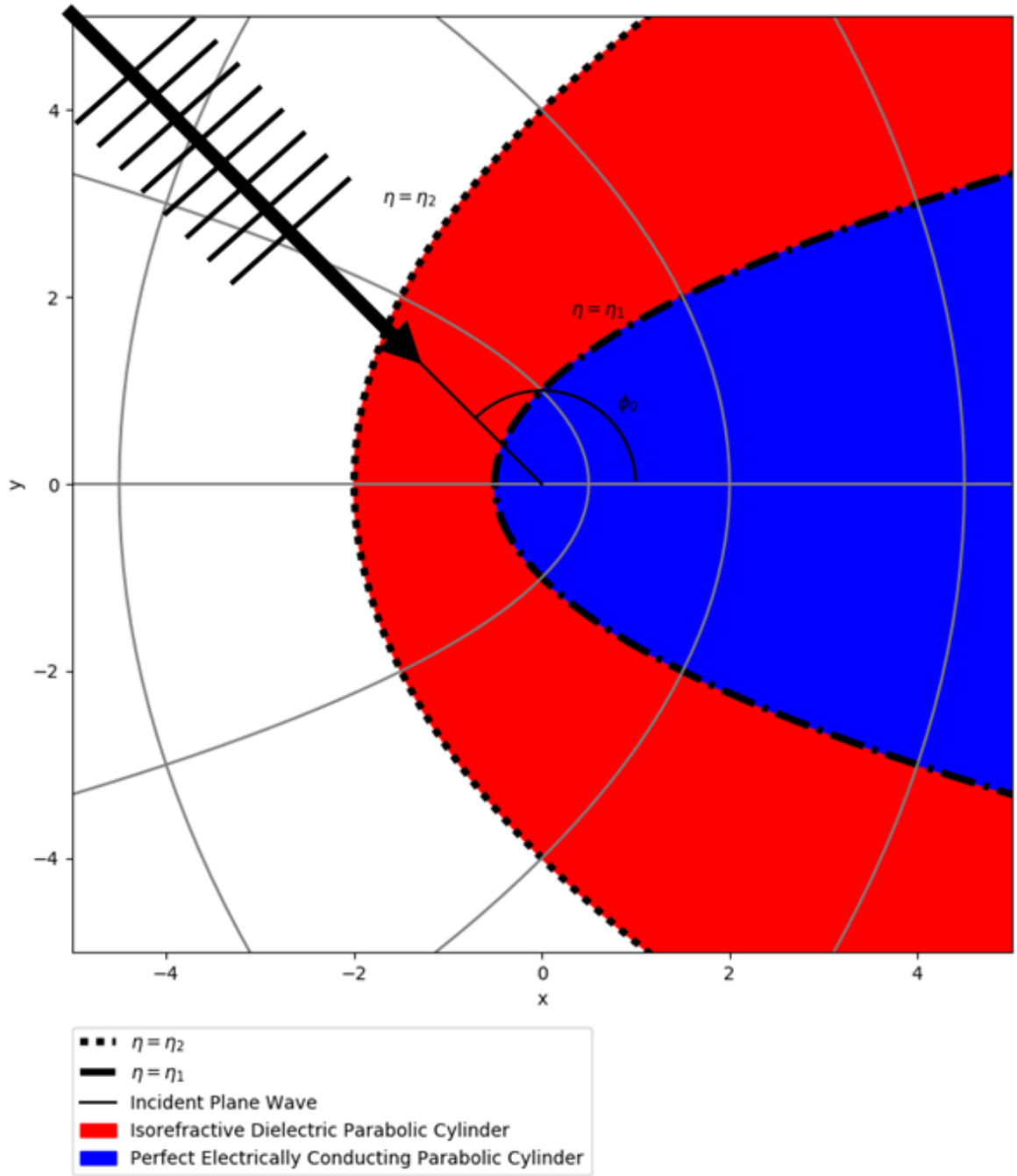


Figure 2: Geometry setup of the scattering problem

1.2.3 Circular Cylinder to Parabolic Cylinder Coordinates

An additional relation that will help us in evaluating our problem in the far-field is to consider the relationship between the parabolic cylindrical geometry and the circular cylindrical geometry. From Cartesian coordinates to circular cylindrical coordinates, we make the standard conversion

$$x = \rho \cos \phi \quad (1.18)$$

$$y = \rho \sin \phi$$

$$z = z.$$

Making these substitutions in the relations derived in 1.2.1 for η and ξ , we find

$$\eta^2 = \rho \sin \phi \tan \frac{\phi}{2} \quad (1.19)$$

$$\xi^2 = \rho(1 + \cos \phi).$$

Further simplification of these expressions leads us to

$$\eta^2 = 2\rho \sin^2 \frac{\phi}{2} \quad (1.20)$$

$$\xi^2 = 2\rho \cos^2 \frac{\phi}{2}$$

or even more simply

$$\begin{aligned}\eta &= \sqrt{2\rho} \sin \frac{\phi}{2} \\ \xi &= \sqrt{2\rho} \cos \frac{\phi}{2}.\end{aligned}\tag{1.21}$$

The simplicity of these expressions will help us later.

1.3 Calculus and the Parabolic Cylinder Functions

Let us consider how vector calculus properties convert from a Cartesian coordinate system to our parabolic cylinder coordinate system. First, consider the curl of a field in the parabolic cylinder coordinate system. Given a function of orthogonal coordinates $\vec{U}(\eta, \xi, z)$, the curl of the function, $\vec{\nabla} \times \vec{U}$ is (36)

$$\begin{aligned}\vec{\nabla} \times \vec{U} &= \left(\frac{1}{\sqrt{\eta^2 + \xi^2}} \frac{\partial U_z}{\partial \xi} - \frac{\partial U_\xi}{\partial z} \right) \hat{\eta} - \left(\frac{1}{\sqrt{\eta^2 + \xi^2}} \frac{\partial U_z}{\partial \eta} - \frac{\partial U_\eta}{\partial z} \right) \hat{\xi} \\ &\quad + \frac{1}{\eta^2 + \xi^2} \left(\frac{\partial \sqrt{\eta^2 + \xi^2} U_\eta}{\partial \xi} - \frac{\partial \sqrt{\eta^2 + \xi^2} U_\xi}{\partial \eta} \right) \hat{z}.\end{aligned}\tag{1.22}$$

This property we will find necessary in calculating our propagating magnetic fields from electric fields and vice versa.

Now in any radiation problem, we require that our field at all points satisfy the Helmholtz equation (37), using again our arbitrary function $\vec{U}(\eta, \xi, z)$

$$(\vec{\nabla}^2 + k^2)\vec{U} = 0.\tag{1.23}$$

By an ordinary change of variable, we find that in our parabolic cylinder coordinate system, the Helmholtz equation can be expressed in the form of (38)

$$\frac{\partial^2 \vec{U}}{\partial \xi^2} + \frac{\partial^2 \vec{U}}{\partial \eta^2} + k^2(\xi^2 + \eta^2)\vec{U} = 0. \quad (1.24)$$

By separation of variables, the above equation takes the form (39) (40)

$$\frac{d^2 y}{d\alpha^2} + \left(n + \frac{1}{2} + \frac{\alpha^2}{4}\right)y = 0. \quad (1.25)$$

Equation 1.25 above has solutions known as *parabolic cylinder functions*, or *Weber-Hermite functions*. These solutions take the form (38)

$$y = D_n(\zeta) \quad (1.26)$$

where the expression $D_n(\zeta)$ takes the form

$$D_n(\zeta) = e^{-\zeta^2/4} 2^{-n/2} H_n(2^{-1/2}\zeta) \quad (1.27)$$

where $H_n(2^{-1/2}\zeta)$ is the Hermite polynomial of degree n . The full solutions to Equation 1.24 are written as products of the form

$$\vec{U}(\eta, \xi, z) = D_n(-\xi e^{i\pi/4}\sqrt{2k})D_n(\eta e^{-i\pi/4}\sqrt{2k}) \quad (1.28)$$

$$\vec{U}(\eta, \xi, z) = D_n(-\xi e^{i\pi/4}\sqrt{2k})D_{-n-1}(\eta e^{i\pi/4}\sqrt{2k}) \quad (1.29)$$

These parabolic cylinder functions are of vital importance to us as they will be used to construct explicit analytic expressions for our wave functions in the parabolic cylinder coordinate system.

1.4 Boundary Value Problems Background

Many problems in electrodynamics are solved through the application of boundary value conditions. That is, at the boundary between two different types of media, we apply some sort of constraint to our fields at these interfaces. Applying boundary conditions allows us to solve a general system of equations.

First, let us state the boundary value condition for an electric field at the surface of a PEC:

$$\vec{E} - (\vec{E} \cdot \hat{n})\hat{n} = 0. \quad (1.30)$$

This equation states that the electric field at the interface of a PEC has only components normal to the surface, and the tangential components sum to 0.

At the boundary between two materials with different dielectric properties, e.g. at the interface between two isorefractive materials, the tangential components of our electric and magnetic fields must obey the following boundary value conditions:

$$\vec{E}_{1\parallel} = \vec{E}_{2\parallel} \tag{1.31}$$

$$\vec{H}_{1\parallel} = \vec{H}_{2\parallel}. \tag{1.32}$$

These constraints will be applied repeatedly throughout this work.

CHAPTER 2

ANALYTIC SOLUTIONS

After laying down the fundamental mathematical and physical groundwork, we are ready to take on the task of finding the exact analytic solution to the problem of a plane wave scattering from a PEC parabolic cylinder sheathed in confocal isorefractive material. We will consider two polarizations; the first with the electric field polarized parallel to the z -axis, which we shall refer to as *Electric Polarization*, and the second with the magnetic field polarized parallel to the z -axis, which we shall refer to as *Magnetic Polarization*. Moving forward, we will use this naming convention to refer to the two configurations.

2.1 Plane Wave Source - Electric Polarization

Consider a plane wave incident on the convex side of our parabolic cylinders. In Cartesian coordinates, the general expression for a plane wave is

$$\vec{E}(\vec{r}, t) = E_0 e^{i(\vec{k} \cdot \vec{r} - \omega t)}. \quad (2.1)$$

In our problem, the plane wave propagates normal to the z -axis, and the electric field is polarized parallel to it. The incident wave makes an angle ϕ_0 with the positive x -axis, as in Figure 2.

We can write this expression more explicitly as

$$\vec{E}^i(x, y) = e^{ik_2(x \cos \phi_0 + y \sin \phi_0)} \hat{z} \quad (2.2)$$

where we have omitted the time dependence $e^{-i\omega t}$, replaced \vec{k} with its magnitude in the exterior region, k_2 , and assumed the magnitude of the field $E_0 = 1$. The superscript i on $\vec{E}^i(x, y)$ indicates that this is the incident field, and when used in this manner should not be confused with the imaginary unit i . Later, we shall consider the imaginary parts of fields, at which point it will be explicitly stated that we are considering the imaginary component. We will use k in the usual sense as

$$k_2 = \omega \sqrt{\epsilon_2 \mu_2} = \omega \sqrt{\epsilon_1 \mu_1} = k_1 = k \quad (2.3)$$

where here we are applying the isorefractive condition. Using the notation of (2) and (1) we can express the incident Parabolic Cylindrical Wave Function (PCF) in the region $\eta > \eta_2$ as

$$\vec{E}_2^i(\eta, \xi) = \frac{1}{\sin \frac{\Phi_0}{2}} \sum_{n=0}^{\infty} \frac{(-i \cot \frac{\Phi_0}{2})^n}{n!} D_n(-\xi e^{i\pi/4} \sqrt{2k}) D_n(\eta e^{-i\pi/4} \sqrt{2k}) \hat{z} \quad (2.4)$$

where it may be useful to recall from 1.3 that the product of D_n satisfies the Helmholtz equation in our problem geometry, just as Equation 2.2 solves the Helmholtz equation in Cartesian coordinates. Expressing a general equation for a wave, followed by applying boundary value conditions to extract the specific form of the solution, is the usual path to solving these types of problems. Our next step is to express the scattered electric field in the region $\eta > \eta_2$ as

$$\vec{E}_2^s(\eta, \xi) = \frac{1}{\sin \frac{\Phi_0}{2}} \sum_{n=0}^{\infty} \frac{(-i \cot \frac{\Phi_0}{2})^n}{n!} a_n D_n(-\xi e^{i\pi/4} \sqrt{2k}) D_{-n-1}(\eta e^{i\pi/4} \sqrt{2k}) \hat{z} \quad (2.5)$$

We see here that the scattered, outbound wave is described by the product of D_{-n-1} and D_n .

The total electric field in region two is expressed as the superposition of these two fields, i.e.

$$\vec{E}_2^{\text{tot}}(\eta, \xi) = \frac{1}{\sin \frac{\phi_0}{2}} \sum_{n=0}^{\infty} \frac{(-i \cot \frac{\phi_0}{2})^n}{n!} D_n(-\xi e^{i\pi/4} \sqrt{2k}) [D_n(\eta e^{-i\pi/4} \sqrt{2k}) + a_n D_{-n-1}(\eta e^{i\pi/4} \sqrt{2k})] \hat{z}. \quad (2.6)$$

In the sheath region, for $\eta_1 < \eta < \eta_2$ we first write our “right-moving”, initially transmitted wave as

$$\vec{E}_1^i(\eta, \xi) = \frac{1}{\sin \frac{\phi_0}{2}} \sum_{n=0}^{\infty} \frac{(-i \cot \frac{\phi_0}{2})^n}{n!} b_n D_n(-\xi e^{i\pi/4} \sqrt{2k}) D_n(\eta e^{-i\pi/4} \sqrt{2k}) \hat{z} \quad (2.7)$$

and the wave reflected off the impenetrable surface in $\eta = \eta_1$ is expressed as:

$$\vec{E}_1^s(\eta, \xi) = \frac{1}{\sin \frac{\phi_0}{2}} \sum_{n=0}^{\infty} \frac{(-i \cot \frac{\phi_0}{2})^n}{n!} c_n D_n(-\xi e^{i\pi/4} \sqrt{2k}) D_{-n-1}(\eta e^{i\pi/4} \sqrt{2k}) \hat{z} \quad (2.8)$$

So we can now similarly write our expression for the total electric field inside the sheath region, region 1, as

$$\vec{E}_1^{\text{tot}}(\eta, \xi) = \frac{1}{\sin \frac{\phi_0}{2}} \sum_{n=0}^{\infty} \frac{(-i \cot \frac{\phi_0}{2})^n}{n!} D_n(-\xi e^{i\pi/4} \sqrt{2k}) [b_n D_n(\eta e^{-i\pi/4} \sqrt{2k}) + c_n D_{-n-1}(\eta e^{i\pi/4} \sqrt{2k})] \hat{z} \quad (2.9)$$

We take special care now to point out that we have been able to use a single expression for k because we have applied the isorefractive condition. As these explicit expressions are a bit

cumbersome, let's work to further simplify these where possible. We will make the following substitutions:

$$\begin{aligned}\sigma &= \sin \frac{\phi_0}{2} & \kappa &= \cot \frac{\phi_0}{2} \\ \gamma^+ &= e^{i\pi/4}\sqrt{2k} & \gamma^- &= e^{-i\pi/4}\sqrt{2k}\end{aligned}\tag{2.10}$$

Using these substitutions, we write our expressions for the total electric field as

$$\vec{E}_2^{\text{tot}}(\eta, \xi) = \frac{1}{\sigma} \sum_{n=0}^{\infty} \frac{(-i\kappa)^n}{n!} D_n(-\xi\gamma^+) [D_n(\eta\gamma^-) + a_n D_{-n-1}(\eta\gamma^+)] \hat{z} \tag{2.11}$$

$$\vec{E}_1^{\text{tot}}(\eta, \xi) = \frac{1}{\sigma} \sum_{n=0}^{\infty} \frac{(-i\kappa)^n}{n!} D_n(-\xi\gamma^+) [b_n D_n(\eta\gamma^-) + c_n D_{-n-1}(\eta\gamma^+)] \hat{z} \tag{2.12}$$

We can easily derive the expression for \vec{H} from \vec{E} as done in (37) using the relation

$$\vec{\nabla} \times \vec{E} = -i\omega\mu\vec{H} \tag{2.13}$$

Using the definition of the curl in parabolic cylindrical coordinates, defined in Equation 1.22, we are thus able to write the expression for the \vec{H} fields as

$$\vec{H}_2(\eta, \xi) = \frac{1}{-i\omega\mu_2q} \frac{1}{\sigma} \sum_{n=0}^{\infty} \frac{(-i\kappa)^n}{n!} \left\{ \gamma^+ D'_n(-\xi\gamma^+) [D_n(\eta\gamma^-) + a_n D_{-n-1}(\eta\gamma^+)] \hat{\eta} \right. \quad (2.14)$$

$$\left. - D_n(-\xi\gamma^+) [\gamma^- D'_n(\eta\gamma^-) + \gamma^+ a_n D'_{-n-1}(\eta\gamma^+)] \hat{\xi} \right\}$$

$$\vec{H}_1(\eta, \xi) = \frac{1}{-i\omega\mu_1q} \frac{1}{\sigma} \sum_{n=0}^{\infty} \frac{(-i\kappa)^n}{n!} \left\{ \gamma^+ D'_n(-\xi\gamma^+) [b_n D_n(\eta\gamma^-) + c_n D_{-n-1}(\eta\gamma^+)] \hat{\eta} \right. \quad (2.15)$$

$$\left. - D_n(-\xi\gamma^+) [\gamma^- b_n D'_n(\eta\gamma^-) + \gamma^+ c_n D'_{-n-1}(\eta\gamma^+)] \hat{\xi} \right\}$$

where we have used the substitution $q = \sqrt{\eta^2 + \xi^2}$ and the prime indicates the derivative of the function with respect to η or ξ , respectively. These equations represent the full expression of the magnetic fields in our problem space. Our next step will be to simplify these expressions and apply boundary value conditions. We will write the expressions in a way that is more interchangeable with the conventions used in (2), specifically expressing the constant in front of

the summation in terms of the inverse impedance of each material Y as defined in Equation 1.4 through the following relations

$$\omega = \frac{k}{\sqrt{\epsilon\mu}} \quad (2.16)$$

$$\frac{1}{-i\omega\mu q}\gamma^+ = \frac{1}{-i\omega\mu q}e^{i\pi/4}\sqrt{2k} \quad (2.17)$$

$$= \frac{\sqrt{2k}\sqrt{\epsilon\mu}}{-ik\mu q}e^{i\pi/4} \quad (2.18)$$

$$= \frac{\sqrt{2\epsilon}}{-i\sqrt{k\mu}q}e^{i\pi/4} \quad (2.19)$$

$$= \frac{i\sqrt{2}}{\sqrt{k}q}Ye^{i\pi/4} \quad (2.20)$$

Thus

$$\begin{aligned} \vec{H}_2(\eta, \xi) = \frac{i\sqrt{2}Y_2}{\sqrt{k}q\sigma} \sum_{n=0}^{\infty} \frac{(-ik)^n}{n!} \left\{ e^{i\pi/4}D'_n(-\xi\gamma^+) [D_n(\eta\gamma^-) + a_n D_{-n-1}(\eta\gamma^+)] \hat{\eta} \right. \\ \left. - D_n(-\xi\gamma^+) [e^{-i\pi/4}D'_n(\eta\gamma^-) + e^{i\pi/4}a_n D'_{-n-1}(\eta\gamma^+)] \hat{\xi} \right\} \end{aligned} \quad (2.21)$$

$$\begin{aligned} \vec{H}_1(\eta, \xi) = \frac{i\sqrt{2}Y_1}{\sqrt{k}q\sigma} \sum_{n=0}^{\infty} \frac{(-ik)^n}{n!} \left\{ e^{i\pi/4}D'_n(-\xi\gamma^+) [b_n D_n(\eta\gamma^-) + c_n D_{-n-1}(\eta\gamma^+)] \hat{\eta} \right. \\ \left. - D_n(-\xi\gamma^+) [e^{-i\pi/4}b_n D'_n(\eta\gamma^-) + e^{i\pi/4}c_n D'_{-n-1}(\eta\gamma^+)] \hat{\xi} \right\} \end{aligned} \quad (2.22)$$

We turn our attention now to the application of our boundary value conditions. Let's start by applying the condition used in Equation 1.30 at the PEC interface where $\eta = \eta_1$, we find:

$$b_n D_n(\eta_1 \gamma^-) + c_n D_{-n-1}(\eta_1 \gamma^+) = 0 \quad (2.23)$$

At the interface $\eta = \eta_2$, we only need concern ourself with the components of the electric and magnetic fields tangential to the parabolic cylinder surface, specifically we ignore the components of \vec{H} in the $\hat{\eta}$ direction. Utilizing the constraints specified in Equation 1.31, we specify the continuity of the tangential electric field at the interface $\eta = \eta_2$ by

$$D_n(\eta_2 \gamma^-) + a_n D_{-n-1}(\eta_2 \gamma^+) = b_n D_n(\eta_2 \gamma^-) + c_n D_{-n-1}(\eta_2 \gamma^+) \quad (2.24)$$

Similarly, constraining the continuity of the tangential magnetic field at the interface $\eta = \eta_2$:

$$Y_2 [e^{-i\pi/4} D'_n(\eta_2 \gamma^-) + e^{i\pi/4} a_n D'_{-n-1}(\eta_2 \gamma^+)] = Y_1 [e^{-i\pi/4} b_n D'_n(\eta_2 \gamma^-) + e^{i\pi/4} c_n D'_{-n-1}(\eta_2 \gamma^+)] \quad (2.25)$$

We now have a system of three equations with three unknown coefficients, and this can be solved. From Equation 2.23

$$\boxed{b_n = -c_n \frac{D_{-n-1}(\eta_1 \gamma^+)}{D_n(\eta_1 \gamma^-)}}. \quad (2.26)$$

Using this relation, rewrite Equation 2.24

$$\boxed{a_n = \frac{1}{D_{-n-1}(\eta_2\gamma^+)} c_n \left(D_{-n-1}(\eta_2\gamma^+) - \frac{D_{-n-1}(\eta_1\gamma^+)}{D_n(\eta_1\gamma^-)} D_n(\eta_2\gamma^-) \right) - \frac{D_n(\eta_2\gamma^-)}{D_{-n-1}(\eta_2\gamma^+)}. \quad (2.27)}$$

Both these relations can be used to rewrite Equation 2.25

$$\begin{aligned} Y_2 \left\{ e^{-i\pi/4} D'_n(\eta_2\gamma^-) \right. & \quad (2.28) \\ & + e^{i\pi/4} \left[\frac{c_n}{D_{-n-1}(\eta_2\gamma^+)} \left(D_{-n-1}(\eta_2\gamma^+) - \frac{D_{-n-1}(\eta_1\gamma^+)}{D_n(\eta_1\gamma^-)} D_n(\eta_2\gamma^-) \right) - \frac{D_n(\eta_2\gamma^-)}{D_{-n-1}(\eta_2\gamma^+)} \right] D'_{-n-1}(\eta_2\gamma^+) \Big\} \\ & = Y_1 \left\{ -e^{-i\pi/4} \left(c_n \frac{D_{-n-1}(\eta_1\gamma^+)}{D_n(\eta_1\gamma^-)} \right) D'_n(\eta_2\gamma^-) + e^{i\pi/4} c_n D'_{-n-1}(\eta_2\gamma^+) \right\}. \end{aligned}$$

Multiplying both sides of the above equation by $e^{-i\pi/4}$ and rearranging yields the full analytic expression for c_n :

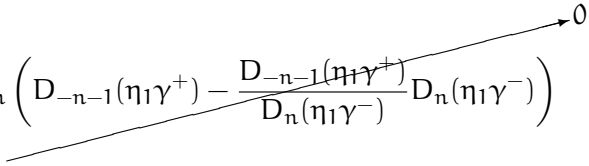
$$\boxed{c_n = Y_2 \left[i D'_n(\eta_2\gamma^-) + \frac{D_n(\eta_2\gamma^-)}{D_{-n-1}(\eta_2\gamma^+)} D'_{-n-1}(\eta_2\gamma^+) \right] \left[Y_2 \frac{D'_{-n-1}(\eta_2\gamma^+)}{D_{-n-1}(\eta_2\gamma^+)} \left(D_{-n-1}(\eta_2\gamma^+) - \frac{D_{-n-1}(\eta_1\gamma^+)}{D_n(\eta_1\gamma^-)} D_n(\eta_2\gamma^-) \right) - i Y_1 \frac{D_{-n-1}(\eta_1\gamma^+)}{D_n(\eta_1\gamma^-)} D'_n(\eta_2\gamma^-) - Y_1 D'_{-n-1}(\eta_2\gamma^+) \right]^{-1} \quad (2.29)}$$

Now, with full analytic expressions we can compute our coefficients, investigate their properties in asymptotic limits, and evaluate the scattered fields they produce.

2.2 Simple PEC Scattering Limit

As a check on our work thus far, consider the limiting case when $\eta_2 \rightarrow \eta_1$, i.e. when the thickness of the isorefractive sheath vanishes. In this limit we expect to recover the solution of

a plane wave scattering off of a PEC parabolic cylinder. This is the exact problem presented in (1), and should prove a good check on our work. In the far field, we are interested in the behavior of the expansion coefficient a_n . We start by considering our expression for a_n in Equation 2.27, and we replace η_2 by η_1

$$a_n = \frac{1}{D_{-n-1}(\eta_1 \gamma^+)} c_n \left(D_{-n-1}(\eta_1 \gamma^+) - \frac{D_{-n-1}(\eta_1 \gamma^+)}{D_n(\eta_1 \gamma^-)} D_n(\eta_1 \gamma^-) \right) - \frac{D_n(\eta_1 \gamma^-)}{D_{-n-1}(\eta_1 \gamma^+)} \quad (2.30)$$


Thus any dependence of a_n on c_n disappears, and we are left with

$$a_n = -\frac{D_n(\eta_1 \gamma^-)}{D_{-n-1}(\eta_1 \gamma^+)} \quad (2.31)$$

which exactly matches the equivalent expression in (1).

At this time it is helpful to address the factors of γ^\pm . Recall that these variables contain factors of $e^{\pm i\pi/4}$. Readers of this paper who read our cited works will find that authors differ in their use of the positive or negative exponential within the parabolic cylinder functions. This difference only introduces a half-period difference in phase between authors, and has no impact on final expressions so long as implementation is consistent within a single calculation. It is equivalent to evaluating the complex conjugate of an expression; the end result will not be impacted by choice of plus or minus.

Thus, we have recovered the expression for plane wave scattering from a PEC parabolic cylinder as expected, and with confidence in our methods we will proceed with further analytic study and computation of our results.

2.3 Plane Wave Source - Magnetic Polarization

Following the prescription set forth in 2.1, we again consider the problem a a plane wave incident on the convex side of our cylinder, but with the magnetic field oriented parallel to the z-axis. The plane wave again propagates orthogonal to the z-axis. In Cartesian coordinates, we express the incident wave, omitting the time dependence, as

$$\vec{H}^i(x, y) = e^{-ik_2(x \cos \phi_0 + y \sin \phi_0)} \hat{z} \quad (2.32)$$

where again the superscript i indicates that this is the incident field, and we will use k in the usual sense:

$$k_2 = \omega \sqrt{\epsilon_2 \mu_2} = \omega \sqrt{\epsilon_1 \mu_1} = k_1 = k \quad (2.33)$$

We again express the incident and scattered fields in the region $\eta > \eta_2$ in terms of parabolic cylindrical wave functions:

$$\vec{H}_2^{\text{tot}}(\eta, \xi) = \frac{1}{\sin \frac{\phi_0}{2}} \sum_{n=0}^{\infty} \frac{(-i \cot \frac{\phi_0}{2})^n}{n!} D_n(-\xi e^{i\pi/4} \sqrt{2k}) [D_n(\eta e^{-i\pi/4} \sqrt{2k}) + a_n D_{-n-1}(\eta e^{i\pi/4} \sqrt{2k})] \hat{z} \quad (2.34)$$

And in the region $\eta_1 < \eta < \eta_2$ by

$$\vec{H}_1^{\text{tot}}(\eta, \xi) = \frac{1}{\sin \frac{\phi_0}{2}} \sum_{n=0}^{\infty} \frac{(-i \cot \frac{\phi_0}{2})^n}{n!} D_n(-\xi e^{i\pi/4} \sqrt{2k}) [b_n D_n(\eta e^{-i\pi/4} \sqrt{2k}) + c_n D_{-n-1}(\eta e^{i\pi/4} \sqrt{2k})] \hat{z} \quad (2.35)$$

Again we use the simplifications defined in Equation 2.10, and we write out the simplified expressions as

$$\vec{H}_2^{\text{tot}}(\eta, \xi) = \frac{1}{\sigma} \sum_{n=0}^{\infty} \frac{(-i\kappa)^n}{n!} D_n(-\xi \gamma^+) [D_n(\eta \gamma^-) + a_n D_{-n-1}(\eta \gamma^+)] \hat{z} \quad (2.36)$$

$$\vec{H}_1^{\text{tot}}(\eta, \xi) = \frac{1}{\sigma} \sum_{n=0}^{\infty} \frac{(-i\kappa)^n}{n!} D_n(-\xi \gamma^+) [b_n D_n(\eta \gamma^-) + c_n D_{-n-1}(\eta \gamma^+)] \hat{z}. \quad (2.37)$$

We derive the expression for \vec{E} from \vec{H} as shown in (37) using the relation

$$\vec{E} = \frac{1}{i\omega\epsilon} \vec{\nabla} \times \vec{H} \quad (2.38)$$

Again we use the definition of the curl in parabolic cylindrical coordinates from Equation 1.22, and find \vec{E} as

$$\begin{aligned} \vec{E}_2(\eta, \xi) = \frac{1}{i\omega\epsilon_2q} \frac{1}{\sigma} \sum_{n=0}^{\infty} \frac{(-i\kappa)^n}{n!} \left\{ \gamma^+ D'_n(-\xi\gamma^+) [D_n(\eta\gamma^-) + a_n D_{-n-1}(\eta\gamma^+)] \hat{\eta} \right. \\ \left. - D_n(-\xi\gamma^+) [\gamma^- D'_n(\eta\gamma^-) + \gamma^+ a_n D'_{-n-1}(\eta\gamma^+)] \hat{\xi} \right\} \end{aligned} \quad (2.39)$$

$$\begin{aligned} \vec{E}_1(\eta, \xi) = \frac{1}{i\omega\epsilon_1q} \frac{1}{\sigma} \sum_{n=0}^{\infty} \frac{(-i\kappa)^n}{n!} \left\{ \gamma^+ D'_n(-\xi\gamma^+) [b_n D_n(\eta\gamma^-) + c_n D_{-n-1}(\eta\gamma^+)] \hat{\eta} \right. \\ \left. - D_n(-\xi\gamma^+) [\gamma^- b_n D'_n(\eta\gamma^-) + \gamma^+ c_n D'_{-n-1}(\eta\gamma^+)] \hat{\xi} \right\} \end{aligned} \quad (2.40)$$

where we have again used the substitution $q = \sqrt{\eta^2 + \xi^2}$ and the prime indicates the derivative of the function with respect to η or ξ , respectively. We will further simplify this expression using the definition of intrinsic impedance laid out in Equation 1.3.

$$\omega = \frac{k}{\sqrt{\epsilon\mu}} \quad (2.41)$$

$$\frac{1}{i\omega\epsilon q} \gamma^+ = \frac{\sqrt{2k}}{i\omega\epsilon q} e^{i\pi/4} \quad (2.42)$$

$$= \frac{\sqrt{2k}\sqrt{\epsilon\mu}}{-i\kappa\epsilon q} e^{i\pi/4} \quad (2.43)$$

$$= \frac{\sqrt{2\mu}}{-i\sqrt{k\epsilon}q} e^{i\pi/4} \quad (2.44)$$

$$= \frac{i\sqrt{2}}{\sqrt{k}q} Z e^{i\pi/4} \quad (2.45)$$

Utilizing this relation we simplify our equations for the total electric fields as

$$\begin{aligned} \vec{E}_2(\eta, \xi) = \frac{i\sqrt{2}Z_2}{\sqrt{kq\sigma}} \sum_{n=0}^{\infty} \frac{(-i\kappa)^n}{n!} \left\{ e^{i\pi/4} D'_n(-\xi\gamma^+) [D_n(\eta\gamma^-) + a_n D_{-n-1}(\eta\gamma^+)] \hat{\eta} \right. \\ \left. - D_n(-\xi\gamma^+) [e^{-i\pi/4} D'_n(\eta\gamma^-) + e^{i\pi/4} a_n D'_{-n-1}(\eta\gamma^+)] \hat{\xi} \right\} \end{aligned} \quad (2.46)$$

$$\begin{aligned} \vec{E}_1(\eta, \xi) = \frac{i\sqrt{2}Z_1}{\sqrt{kq\sigma}} \sum_{n=0}^{\infty} \frac{(-i\kappa)^n}{n!} \left\{ e^{i\pi/4} D'_n(-\xi\gamma^+) [b_n D_n(\eta\gamma^-) + c_n D_{-n-1}(\eta\gamma^+)] \hat{\eta} \right. \\ \left. - D_n(-\xi\gamma^+) [e^{-i\pi/4} b_n D'_n(\eta\gamma^-) + e^{i\pi/4} c_n D'_{-n-1}(\eta\gamma^+)] \hat{\xi} \right\} \end{aligned} \quad (2.47)$$

With our fields explicitly expressed, we turn our attention again to the application of our boundary value conditions. We first apply the condition used in Equation 1.30 at the PEC interface where $\eta = \eta_1$ for Equation 2.47, which is more complicated in this scenario than that of 2.1

$$e^{-i\pi/4} b_n D'_n(\eta_1 \gamma^-) + e^{i\pi/4} c_n D'_{-n-1}(\eta_1 \gamma^+) = 0 \quad (2.48)$$

or simplifying further

$$b_n = i c_n \frac{D'_{-n-1}(\eta_1 \gamma^+)}{D'_n(\eta_1 \gamma^-)} \quad (2.49)$$

Utilizing the constraints specified in Equation 1.31, we specify the continuity of the tangential electric field (again, in the $\hat{\xi}$ direction) at the interface $\eta = \eta_2$

$$Z_2 [e^{-i\pi/4} D'_n(\eta_2 \gamma^-) + e^{i\pi/4} a_n D'_{-n-1}(\eta_2 \gamma^+)] = Z_1 [e^{-i\pi/4} b_n D'_n(\eta_2 \gamma^-) + e^{i\pi/4} c_n D'_{-n-1}(\eta_2 \gamma^+)] \quad (2.50)$$

and the continuity of the tangential magnetic field at the interface $\eta = \eta_2$

$$D_n(\eta_2 \gamma^-) + a_n D_{-n-1}(\eta_2 \gamma^+) = b_n D_n(\eta_2 \gamma^-) + c_n D_{-n-1}(\eta_2 \gamma^+) \quad (2.51)$$

Again we have a system of three equations with three unknown coefficients. Using Equation 2.49 in Equation 2.51 we find

$$a_n = \frac{1}{D_{-n-1}(\eta_2 \gamma^+)} c_n \left(D_{-n-1}(\eta_2 \gamma^+) + i \frac{D'_{-n-1}(\eta_1 \gamma^+)}{D'_n(\eta_1 \gamma^-)} D_n(\eta_2 \gamma^-) \right) - \frac{D_n(\eta_2 \gamma^-)}{D_{-n-1}(\eta_2 \gamma^+)} \quad (2.52)$$

and we can use both Equation 2.52 and Equation 2.49 to rewrite Equation 2.50 as:

$$\begin{aligned} & Z_2 \left\{ e^{-i\pi/4} D'_n(\eta_2 \gamma^-) \right. \\ & \left. + e^{i\pi/4} \left[\frac{c_n}{D_{-n-1}(\eta_2 \gamma^+)} \left(D_{-n-1}(\eta_2 \gamma^+) + i \frac{D'_{-n-1}(\eta_1 \gamma^+)}{D'_n(\eta_1 \gamma^-)} D_n(\eta_2 \gamma^-) \right) - \frac{D_n(\eta_2 \gamma^-)}{D_{-n-1}(\eta_2 \gamma^+)} \right] D'_{-n-1}(\eta_2 \gamma^+) \right\} \\ & = Z_1 \left\{ i e^{-i\pi/4} \left(c_n \frac{D'_{-n-1}(\eta_1 \gamma^+)}{D'_n(\eta_1 \gamma^-)} \right) D'_n(\eta_2 \gamma^-) + e^{i\pi/4} c_n D'_{-n-1}(\eta_2 \gamma^+) \right\} \end{aligned} \quad (2.53)$$

Multiplying both sides of the above equation by $e^{-i\pi/4}$ and rearranging yields the full analytic expression for c_n :

$$c_n = Z_2 \left[iD'_n(\eta_2\gamma^-) + \frac{D_n(\eta_2\gamma^-)}{D_{-n-1}(\eta_2\gamma^+)} D'_{-n-1}(\eta_2\gamma^+) \right] \quad (2.54)$$

$$\left[Z_2 \frac{D'_{-n-1}(\eta_2\gamma^+)}{D_{-n-1}(\eta_2\gamma^+)} \left(D_{-n-1}(\eta_2\gamma^+) + i \frac{D'_{-n-1}(\eta_1\gamma^+)}{D'_n(\eta_1\gamma^-)} D_n(\eta_2\gamma^-) \right) \right.$$

$$\left. - Z_1 \frac{D'_{-n-1}(\eta_1\gamma^+)}{D'_n(\eta_1\gamma^-)} D'_n(\eta_2\gamma^-) - Z_1 D'_{-n-1}(\eta_2\gamma^+) \right]^{-1}$$

and so we have derived the full, explicit analytic expression of these coefficients for the magnetic polarization case. As expected, the expressions for the coefficients found here are very similar to those found for the electric polarization case, albeit with a number of PCF functions take with-or-without derivatives. In the sections to follow, there will be plenty of material to consider regarding the electric polarization case alone, and so we leave the magnetic polarization case at this point, having found the exact solution.

CHAPTER 3

NUMERICAL CALCULATIONS - BACKGROUND PROBLEMS

3.1 Introduction

The final goal of this thesis will be to calculate numeric solutions for the problem of the isorefractive sheath, but as a first step towards achieving that goal we will present numeric results for two simpler problem geometries: plane wave scattering from a PEC parabolic cylinder and an isorefractive parabolic cylinder, which were solved in (1) and (2), respectively. These two problems lay the foundation for addressing our ultimate problem, the isorefractive sheath.

In the section to follow, we will present the full steady-state field for each geometry, not just the scattered field. Because of the boundary-value nature of the problem, these plots allow us to easily evaluate the correctness of our calculations. By plotting the field at every point in a two-dimensional area, we start to develop an intuitive understanding for what is happening at the boundary. To further clarify this near-field boundary value behavior, calculations were performed for electric fields with wavelengths on the same order as the separation distance between the parabolic cylinders. This allowed for observing the system with fine granularity. It also may be helpful to address one of our limitations in calculating our fields in this section. In every calculation, the fields are given as a sum over $n = 0 \rightarrow \infty$. The impact of this is that the contribution to the full field expressions from higher orders of n is more apparent as the incident plane wave deviates from $\phi_0 = \pi$. Said another way, our expressions converge

quickly when ϕ_0 is very close to π . This relation was recognized in (3), and we will address the general convergence behavior of these sums in much greater depth in chapter 4. At the moment, because we are interested in the correctness of our boundary value calculations for these simpler geometries, we will address only problems where $\phi_0 = \pi$.

3.2 PEC Scattering

The simplest geometry to plot, and the first scenario that formed the basis of our work, is that of an electric polarized plane wave scattering from a PEC parabolic cylinder. This is the problem tackled in (1), and we showed in 2.2 that our problem (the isorefractive sheath) converges to the PEC case in the limit when the sheath thickness approaches zero. Perhaps the most important advantage of tackling this problem is that it allows us to easily evaluate the accuracy of calculations at the boundary conditions, in this case at the interface with a PEC. We expect that the tangential components of our electric field will vanish at the interface, or in the case of a z-polarized incident electric field, we expect the total electric field to be zero at the boundary.

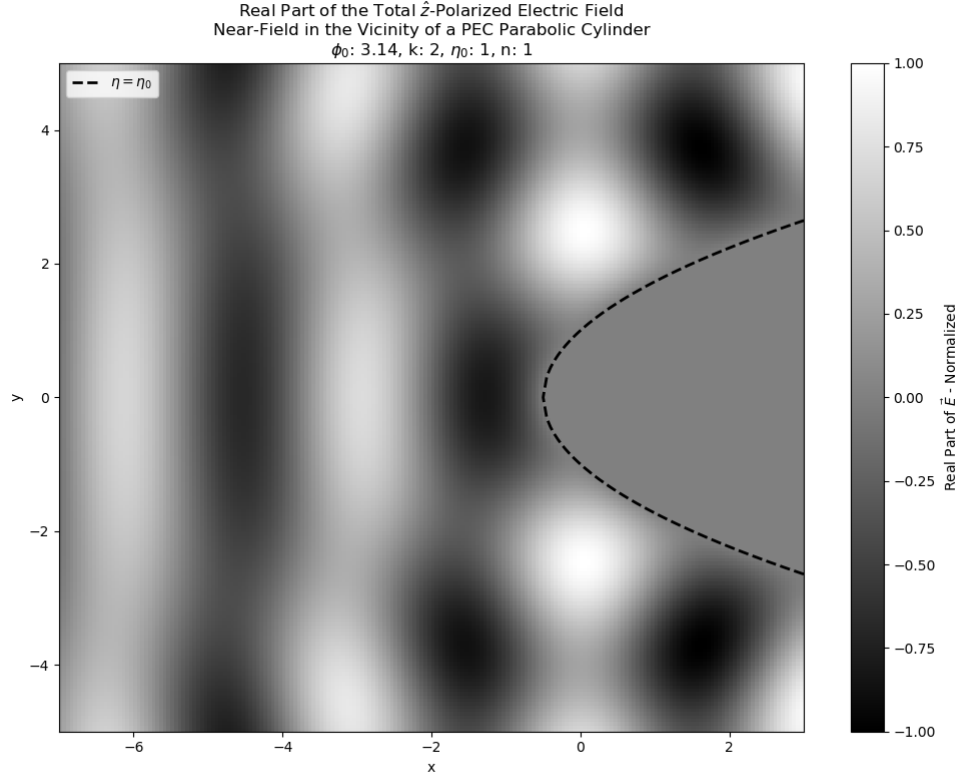


Figure 3: Near-field electric field for a PEC parabolic cylinder

We see in Figure 3 a plot of the complete near-field electric field in the vicinity of the PEC parabolic cylinder. By inspection, it appears that the electric field along the boundary vanishes, as expected. Note as well the oscillatory behavior of the field in the near-field, and how this differs from a plane wave in a vacuum. This is our first interesting glimpse of field behavior in

a parabolic cylinder scattering problem. Figure 4 looks closely at the specific behavior of the field along the x-axis. As expected, at the boundary with the PEC, both the real and imaginary parts of the electric field go to zero. Outside of the boundary, we see the oscillatory nature of the field very clearly.

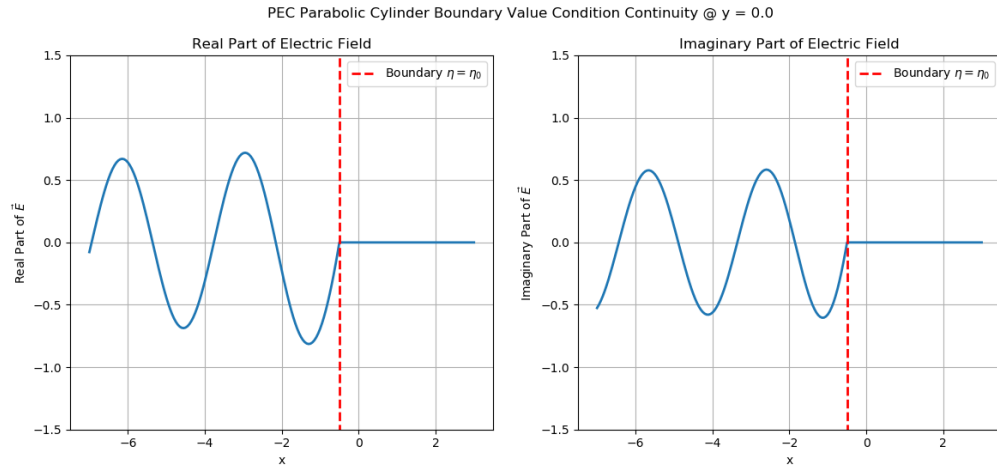


Figure 4: Boundary value condition for a PEC parabolic cylinder

3.3 Isorefractive Scattering

Consider now the similar problem of a plane wave scattering from an isorefractive parabolic cylinder. Recall that this problem laid down the basis of our second application of boundary

conditions, i.e at the isorefractive interface. This is the problem tackled in (2). Again, we first present a plot of the near-field normalized electric field in Figure 5.

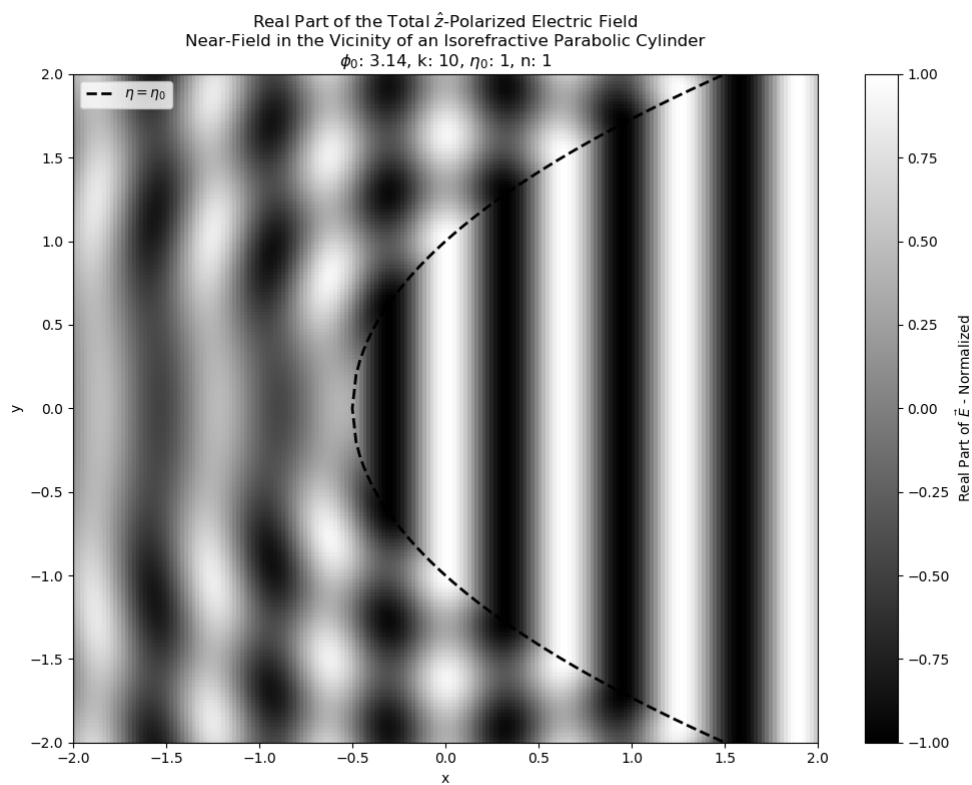


Figure 5: Near-field electric field for an isorefractive parabolic cylinder

Again, we see the oscillatory behavior of the field outside of the parabolic cylinder, but notice now that the plane wave has propagated into the interior of the parabolic cylinder and continues on as a plane-wave. In comparison to Figure 3, we see here that the electric field at the interface is not equal to zero, but is continuous with the fields on the inside.

Now consider the continuity of the electric field across the isorefractive interface, as exhibited in Figure 6

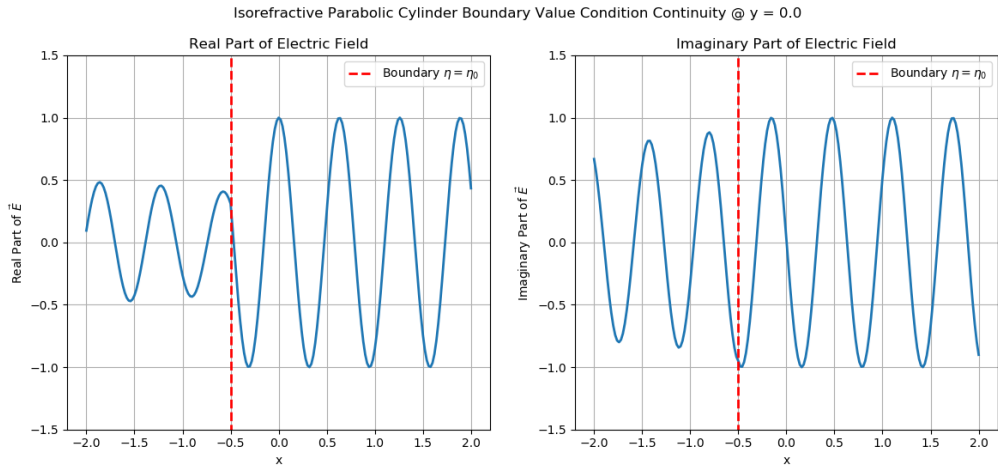


Figure 6: Boundary value condition for an isorefractive parabolic cylinder

We thus see that both the real and imaginary components of the electric field are continuous across the interface, as expected.

CHAPTER 4

NUMERICAL CALCULATIONS - ISOREFRACTIVE SHEATH

4.1 Introduction

In the previous section, we showed that our boundary value calculations yield consistent results for the total field in the near-field region for simple geometries. Now, we aim to take the tools we developed to calculate and plot the fields in the previous chapter, and apply them to our full problem - that of the scattering of a plane wave from a PEC parabolic cylinder embedded in a confocal isorefractive sheath. In a continuation of the analysis of the simpler calculations, we will present the total field in the near-field for this problem geometry. From there, we will venture into deriving expressions for the far-field scattered field. At this point, it will be helpful for us to address some of our computational considerations, and why they are important and must be considered when calculating fields in this problem geometry. We will take a deep dive into the convergence of the infinite series used to describe our fields, and finally we will consider the plots of some scattered fields from our geometry. Before wrapping up this chapter, we will say a few words about the software used to perform our calculations.

4.2 Near-Field Simulation

After the difficult task of deriving our analytic solutions, we are finally ready to calculate some numeric solutions to our problem, the isorefractive sheath. We begin by observing the calculated near-field electric field for our problem using similar input parameters as in chapter

3. In this case, as with others, a number of variables were set to arbitrary values, only chosen to emphasize the behavior of the calculated fields in the vicinity of the boundary interfaces. Additionally, we chose parameters to set the separation distance between the interfaces η_1 and η_2 along the x-axis to be equal to fractions of the wavelength λ . In this case, shown in Figure 7, we chose the distance to be $\frac{7\lambda}{4}$.

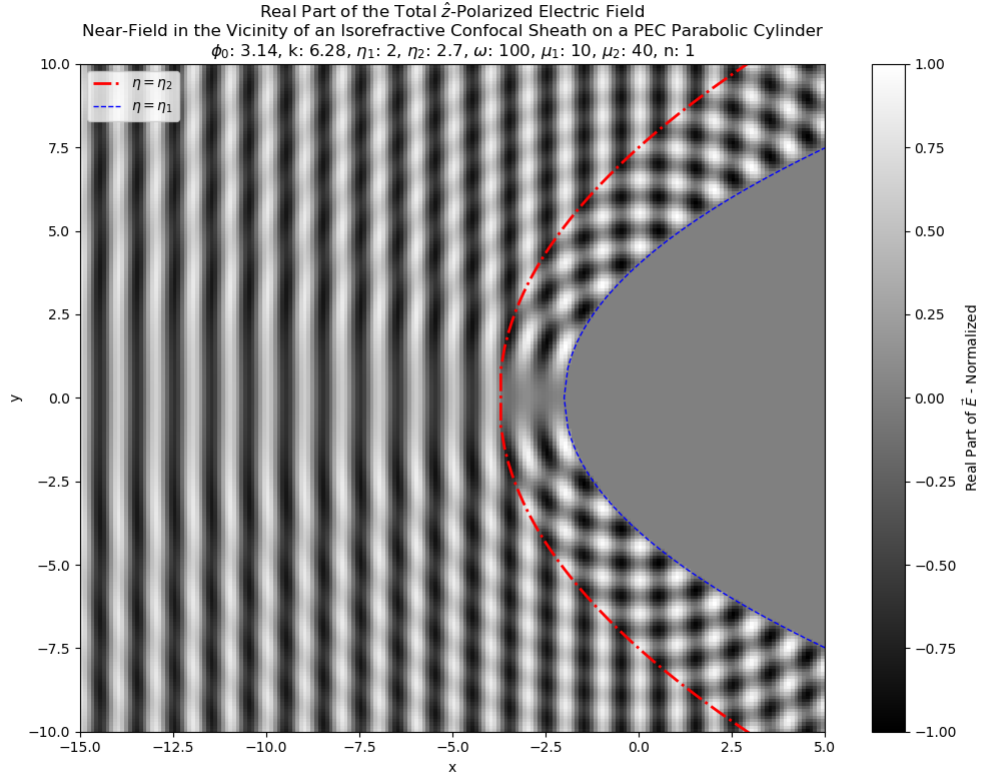


Figure 7: Near-field electric field for an isorefractive sheath of width $\frac{7\lambda}{4}$

Again, we closely observe the behavior of the electric field, again along the x-axis, as it meets our interfaces, as seen in Figure 8. We see that the field is continuous across the isorefractive boundary, and is equal to 0 at the PEC boundary, exactly as expected.

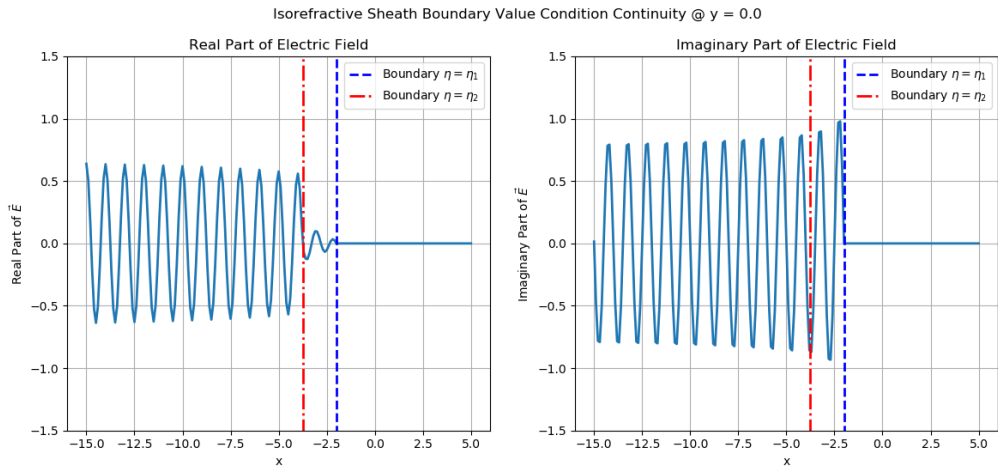
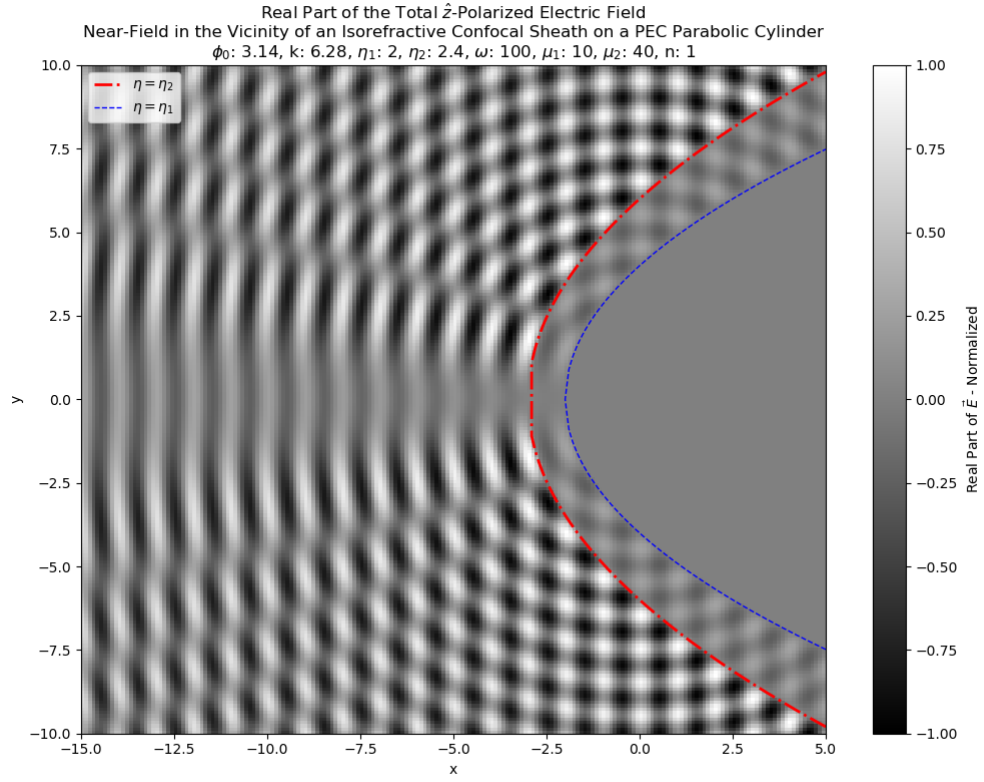
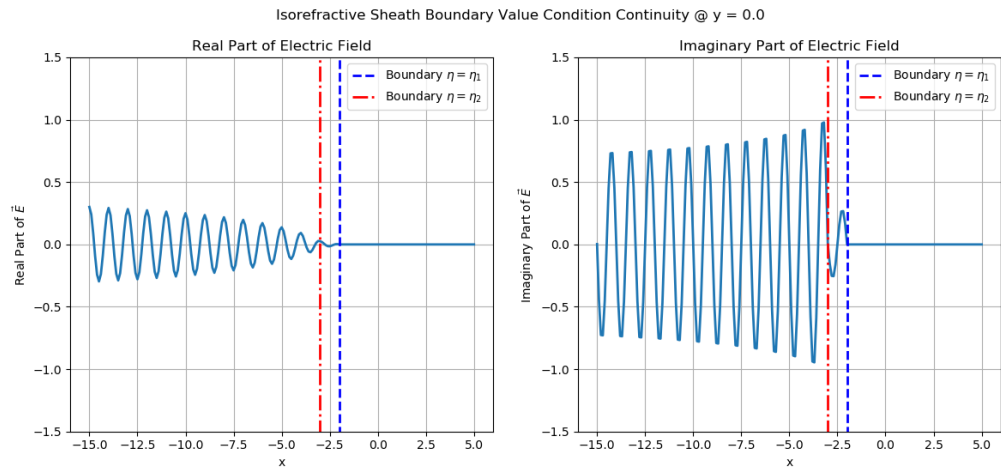


Figure 8: Boundary value condition for an isorefractive sheath of width $\frac{7\lambda}{4}$

The separation distance of the parabolas was chosen as a way to naively implement some conditions that may influence scattering in interesting ways due to emergent interference patterns. In this case, the near-field shows scattering behavior that seems to have little impact on the incident plane wave, except for a reduced intensity along the x-axis.

Figure 9: Near-field electric field for an isorefractive sheath of width λ Figure 10: Boundary value condition for an isorefractive sheath of width λ

Let's compare the results from Figure 7 and Figure 8 with the results in Figure 9 and Figure 10 respectively. Here, we have adjusted the distance between the two parabolic cylinders so that they are now separated by a whole wavelength, λ , but left all other parameters the same. An initial observation shows that the plane-wave like behavior has disappeared, and has been replaced by distinct curves tracing out areas of destructive interference. Again, we see that our boundary value conditions are satisfied, but the behavior near the boundaries is considerably different

These plots hint at interesting far-field behavior that is deserving of further investigation. We will explore some of this far-field behavior, but plots such as these begin to give us a glimpse into the richness of the problem space of our geometry. We naturally begin to ask what behavior we might see for different parabola separation distances, or different intrinsic impedances between the dielectric materials, or different angles of incidence? One hopes that these interesting results may prove useful, whether in evaluating computational software, or in future real-world applications.

4.3 Far-Field Asymptotic Derivation

Now we endeavor to explore the behavior of our problem in the far-field region, i.e. in the region where $\rho \rightarrow \infty$, and we aim to investigate the scattered field as a function of scattering angle ϕ . We will follow, and in some ways expand upon, the prescription set forth in (3). However, the advantage granted to us by evaluating this in an isorefractive sense is that it allows us to analyze the behavior of expressions exactly, whereas (3) was limited to using approximations in evaluating the fields.

We start by considering the explicit expression for the scattered electric field from Equation 2.5 and state again here

$$\vec{E}_2^s(\xi, \eta) = \frac{1}{\sin \frac{\phi_0}{2}} \sum_{n=0}^{\infty} \frac{(-i \cot \frac{\phi_0}{2})^n}{n!} a_n D_n(-\xi e^{i\pi/4} \sqrt{2k}) D_{-n-1}(\eta e^{i\pi/4} \sqrt{2k}) \hat{z}$$

which we now wish to express as a function of scattering angle ϕ . We can convert from parabolic cylindrical coordinates to circular cylindrical coordinates via Equation 1.21 which we restate below¹

$$\begin{aligned} \eta &= \sqrt{2\rho} \sin \frac{\phi}{2} \\ \xi &= \sqrt{2\rho} \cos \frac{\phi}{2} \end{aligned}$$

Let's make the substitutions for η and ξ with their representation in cylindrical coordinates, and again substitute in γ^\pm for clarity

$$\vec{E}_2^s(\rho, \phi) = \frac{1}{\sin \frac{\phi_0}{2}} \sum_{n=0}^{\infty} \frac{(-i \cot \frac{\phi_0}{2})^n}{n!} a_n D_n\left(-\sqrt{2\rho} \cos \frac{\phi}{2} \gamma^+\right) D_{-n-1}\left(\sqrt{2\rho} \sin \frac{\phi}{2} \gamma^+\right) \hat{z} \quad (4.1)$$

¹When $\rho \rightarrow \infty$, we see that ξ and $\eta \rightarrow \infty$ as well. The exception to this is when $\phi = 0$ or 2π forcing $\eta = 0$, or $\phi = \pi$, in which case $\xi = 0$. Fortunately, the PCF functions are continuous across $D_n(0)$ and so this behavior does not impact our analysis.

We now have an expression for the scattered field in cylindrical coordinates. Only the D_n 's are functions of ρ and ϕ , and we can now consider the behavior of this expression when $\rho \rightarrow \infty$. From (40), we have that for a given PCF $D_{-a-\frac{1}{2}}(\zeta)$, when $\zeta \gg a$

$$D_{-a-\frac{1}{2}}(\zeta) = e^{\frac{-\zeta^2}{4}} \zeta^{-a-\frac{1}{2}} \left\{ 1 - \mathcal{O}\left(\frac{1}{\zeta^2}\right) + \mathcal{O}\left(\frac{1}{\zeta^4}\right) \dots \right\} \quad (4.2)$$

which is just a restatement of Equation 1.27 and the relation to Hermite polynomials. We need only consider the highest-ordered exponent in the polynomial as the argument of the function grows to infinity. Thus, dropping fractional terms, we can write D_n as

$$D_{-n-1}(\zeta) \simeq e^{\frac{-\zeta^2}{4}} \zeta^{-n-1} \quad (4.3)$$

$$D_n(\zeta) \simeq e^{\frac{-\zeta^2}{4}} \zeta^n. \quad (4.4)$$

This allows us to express Equation 4.1 in the asymptotic limit as

$$\begin{aligned} \vec{E}_2^s(\rho, \phi) = & \frac{1}{\sin \frac{\phi_0}{2}} \sum_{n=0}^{\infty} \frac{(-i \cot \frac{\phi_0}{2})^n}{n!} \\ & a_n e^{\frac{-(-\sqrt{2\rho} \cos \frac{\phi}{2} \gamma^+)^2}{4}} (-\sqrt{2\rho} \cos \frac{\phi}{2} \gamma^+)^n e^{\frac{-(-\sqrt{2\rho} \sin \frac{\phi}{2} \gamma^+)^2}{4}} (-\sqrt{2\rho} \sin \frac{\phi}{2} \gamma^+)^{-n-1}. \end{aligned} \quad (4.5)$$

A bit of arithmetic allows us to simplify and rearrange this equation, pulling factors independent of n out of the sum

$$\vec{E}_2^s(\rho, \phi) = \frac{e^{\frac{-\rho\gamma^+2}{2}(\cos^2 \frac{\phi}{2} + \sin^2 \frac{\phi}{2})}}{\sin \frac{\phi_0}{2}} \sum_{n=0}^{\infty} \frac{(-i \cot \frac{\phi_0}{2})^n}{n!} a_n \frac{(-\sqrt{2\rho} \cos \frac{\phi}{2} \gamma^+)^n}{(-\sqrt{2\rho} \sin \frac{\phi}{2} \gamma^+)^{n+1}} \quad (4.6)$$

and an additional step of simplification brings us to

$$\vec{E}_2^s(\rho, \phi) = \frac{e^{\frac{-\rho\gamma^+2}{2}}}{-\sqrt{2\rho}\gamma^+ \sin \frac{\phi_0}{2}} \sum_{n=0}^{\infty} \frac{(-i \cot \frac{\phi_0}{2})^n}{n!} a_n \frac{\cot^n(\frac{\phi}{2})}{\sin \frac{\phi}{2}} \quad (4.7)$$

where the entire term $\frac{\cot^n(\frac{\phi}{2})}{\sin \frac{\phi}{2}}$ has intentionally been kept together inside the sum over n as it determines the behavior as a function of scattering angle ϕ . Finally, substituting the gammas back in, we find

$$\vec{E}_2^s(\rho, \phi) = \frac{-e^{-i(\rho k + \pi/4)}}{\sqrt{2\rho k} \sin \frac{\phi_0}{2}} \sum_{n=0}^{\infty} \frac{(-i \cot \frac{\phi_0}{2})^n}{n!} a_n \frac{\cot^n(\frac{\phi}{2})}{\sin \frac{\phi}{2}}. \quad (4.8)$$

We pause here to observe a few things. First, as a simple check of our analysis, we see that the electric field falls off as $\frac{1}{\sqrt{\rho}}$. Thus the radiated power, represented by the Poynting vector \vec{S} , will behave as

$$\vec{S} \propto \vec{E}^2 \propto \frac{1}{\rho} \quad (4.9)$$

which is exactly the $\frac{1}{\rho}$ dependence one expects for a line source or a radiator in two dimensions.

Secondly, we observe that the radiation pattern $F_n(\phi)$ behaves as

$$F_n(\phi) = \frac{\cot^n(\frac{\phi}{2})}{\sin \frac{\phi}{2}} \quad (4.10)$$

This result matches precisely with that of (3). After this asymptotic expansion, we see that our exact expressions for a_n allowed by applying the isorefractive condition will allow us to calculate the exact first-order fields in the far-field. Now, we will evaluate the behavior of Equation 4.8, but before we can do that we will need to consider the sums over n and the convergent properties of these fields.

4.4 Computational Considerations

In order to consider the behavior of our field as a sum over n , we start by defining a scattering coefficient based on Equation 4.8 as

$$\boxed{\Psi_s(\phi) \triangleq \frac{\vec{E}_2^s(\rho, \phi)}{\left(\frac{-e^{-i(\rho k + \pi/4)}}{2\sqrt{\rho k}}\right)} = \frac{1}{\sin \frac{\phi_0}{2}} \sum_{n=0}^{\infty} \frac{(-i \cot \frac{\phi_0}{2})^n}{n!} a_n \frac{\cot^n(\frac{\phi}{2})}{\sin \frac{\phi}{2}}.} \quad (4.11)$$

This scattering coefficient allows us to evaluate the scattered field omitting the rather uninteresting $\frac{1}{\sqrt{\rho}}$ dependence, along with constant $C = \frac{-e^{-i(\rho k + \pi/4)}}{2\sqrt{k}}$ which does not contribute to the shape of total scattered field, but only changes the phase of the entire field as a function of ρ . This scattering coefficient has thus become a function of ϕ alone. Thus, by plotting this scattering coefficient vs. ϕ , we can visualize the scattered field. Before we proceed to plot the scattered field, let's first consider Equation 4.11 with increasing n in a piece-wise manner.

First, let's observe the behavior of the radiation pattern components $F_n(\phi)$. This behavior was investigated in (3), but it is worthwhile to consider again here. Below, we have recreated the plot of $F_n(\phi)$ vs. ϕ from (3) in Figure 11.

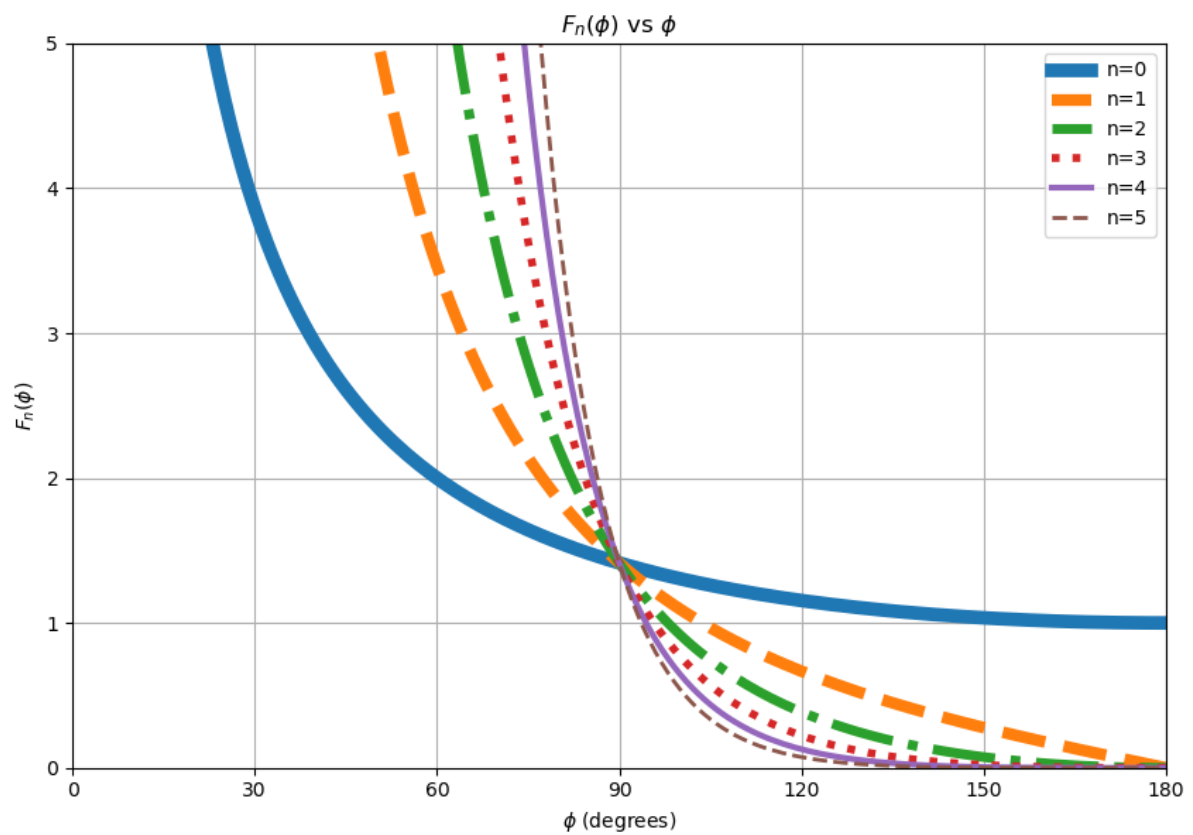


Figure 11: $F_n(\phi)$ vs. ϕ

We observe, just as was found in (3), that for $\phi < 90^\circ$, the radiation pattern increases with increasing n . Note as well that we are presenting the angular dependence in terms of degrees, not radians, both for agreement with (3) and for ease of understanding. In our analysis thus far, we have placed limits on the analysis domain (e.g. we only consider incident waves from $\frac{\pi}{2} \leq \phi_0 \leq \pi$) for convenience, and here we will similarly only consider the scattered field in the region $\frac{\pi}{2} \leq \phi \leq \pi$. The former constraint was applied in (2), and the latter was applied in plotting in (3), although with an additional 10 degree buffer on both the high and low limits. Alternating terms of $F_n(\phi)$ are even or odd functions about the line $\phi = 180^\circ$, and so our domain of $\frac{\pi}{2} \leq \phi \leq \pi$ is sufficient for this analysis.

In our analysis where we limit $\frac{\pi}{2} \leq \phi \leq \pi$, we find that our values of $F_n(\phi)$ either decrease with increasing n , or in the very worst case ($\phi = \frac{\pi}{2}$) remain constant. Thus, if the remaining terms in our sum converge, the contribution from the radiation pattern will converge as well.

Next, let's consider the first part of the asymptotic field equation, which we will call $p_n(\phi_0)$.

$$p_n(\phi_0) = \frac{1}{\sin \frac{\phi_0}{2}} \frac{(-i \cot \frac{\phi_0}{2})^n}{n!} \quad (4.12)$$

$p_n(\phi_0)$ is dependent on n and ϕ_0 only, and so its behavior with increasing n can be easily observed, as shown in Figure 12. We see here that we are in luck, as the magnitude of our terms decrease exponentially, even for an incident angle of 135° . This bodes well for our analysis, as at least one of our terms in each successive iteration of n will become smaller and smaller. Note here that we have plotted the absolute value of each term and have omitted the

sign of each number. This an oscillatory function, and as such alternates between positive and negative terms. In this analysis, we are interested only in the fact that the magnitude of the terms decrease rapidly.

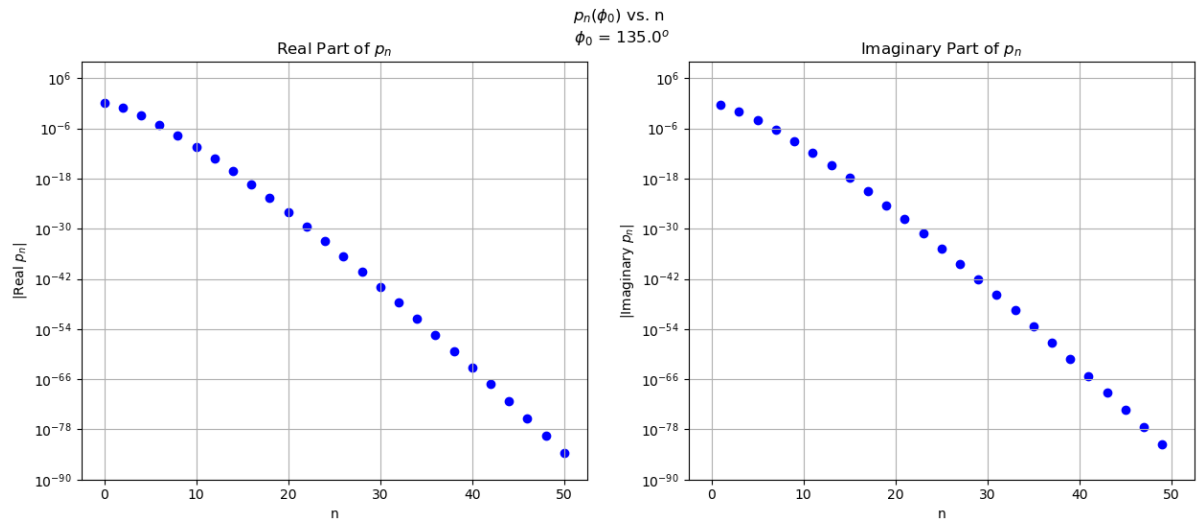


Figure 12: $|p_n(\phi_0)|$ vs. n

Now, let's examine the behavior of our expansion coefficient a_n with increasing n . Again, we emphasize that the calculation of a_n is of paramount importance in this thesis, and so a thorough understanding of the behavior these coefficients with increasing n is vital to success. We have calculated values of a_n for n up to 50 with physical parameters set to reasonable values, and plotted the results in Figure 13. Again, we have plotted the absolute value of the

terms. We see here that a_n grows exponentially, a troubling sign if we hope for our sum to converge. Fortunately, we saw that our series p_n was exponentially decreasing, and the product of the two terms will give us our ultimate behavior.

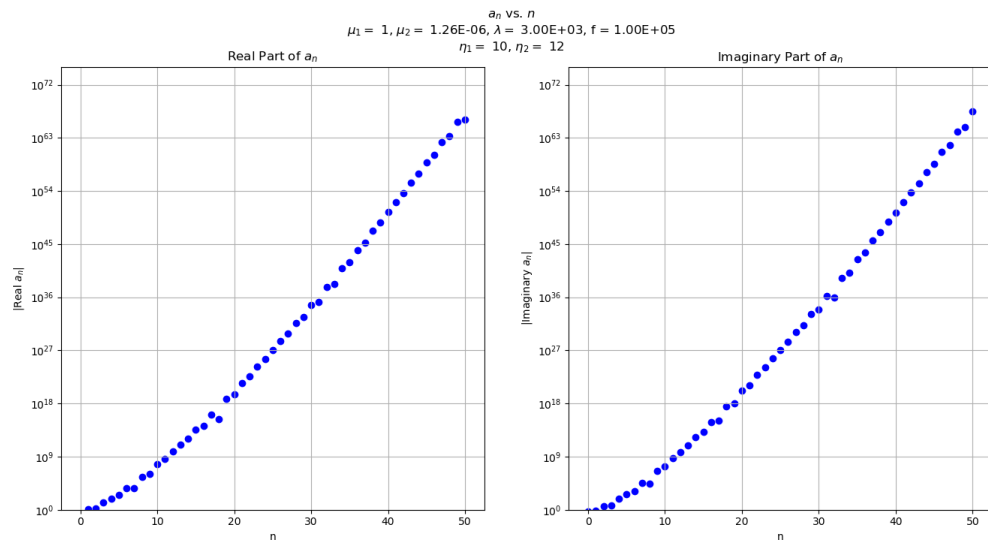


Figure 13: a_n vs. n

It naturally follows that we should go ahead and observe the behavior of the product of a_n and p_n with increasing n , and we see the results of this analysis in Figure 14. Fortunately, we see that for the constants chosen the product of the two terms converges rapidly. For this configuration, summing over 10 iterations of n will provide more than sufficient accuracy. Thus,

we have shown that our infinite sum will converge under accurate, exact calculation of a_n for at least certain sets of input parameters.

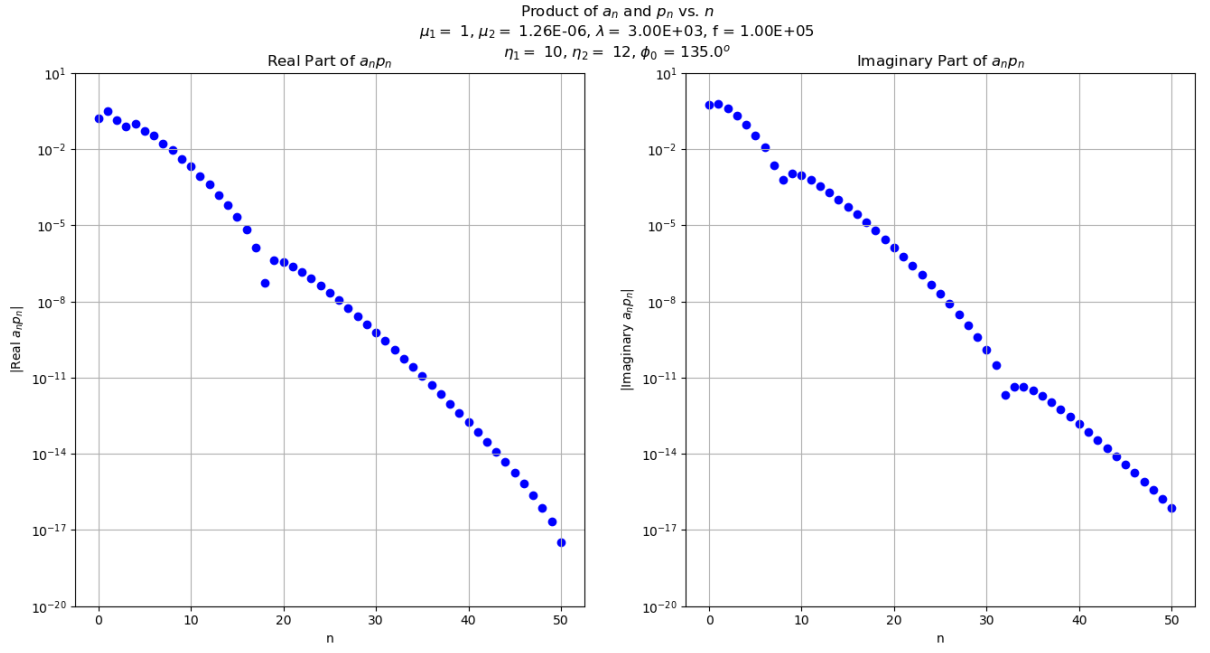


Figure 14: Product of a_n and $p_n(\phi_0)$ vs. n

Now, it may be of interest to the reader to discuss a bit of background concerning the analysis of this sum. If the reader recalls, specific values of variables were chosen to make the near-field analysis more clear and easier to analyze by eye, especially in chapter 3. The values were not chosen with plausible physical constants in mind, but to help interpret the results more

clearly. These placeholder variables were the first values used analysis of the sum over n in the far field. Unfortunately, this led to a problem, in that it appeared at first that the product of a_n and p_n would not converge! Values of these coefficients became very large and very small, respectively, so much so that in some cases they caused overflow errors in the calculation code, and for many terms of n the product kept growing. The detailed analysis of each term was born of necessity in understanding the behavior of the sum. Fortunately, experimentation with different values, and selecting physically plausible values (exactly how “plausible” is up for debate), allowed us to find the numerical solution in Figure 14 which converges rather quickly. Any researcher who sets out to perform similar calculations is warned that the number of terms needed for convergence can vary wildly based on the selection of input parameters, and that special care must be taken in calculating fields to appropriate orders of n to ensure that floating point calculation errors do not influence the final results.

The values used in calculating our fields for the full problem of scattering by an isorefractive parabolic sheath covering a PEC parabolic cylinder are given in Table I. Unit assumptions are based on a single unit in the Cartesian coordinate system being equivalent to one meter, and the angular frequency used is the standard rad/s.

4.5 Convergence of the Infinite Sum

The reader may naturally ask, “How can we be sure that these terms will converge for all input parameters, and the author didn’t simply get lucky with their selection of variable values?” This is a fair question, and one that can be addressed through rigorous analysis of the behavior of the scattering coefficient as the sum over n goes to ∞ . Specifically, as we saw above,

TABLE I: VALUES USED FOR CALCULATING FIELDS

Variable	Value	Description
η_1	10	Surface of PEC
η_2	12	Surface of Sheath
λ	3000(m)	Wavelength of Incident Wave
ω	$6.283 \times 10^5(\text{rad/s})$	Angular Frequency of Incident Wave
k	$2.094 \times 10^{-3}(\text{wavelengths/m})$	Wavenumber
μ_1	1(H/m)	Permeability of the Sheath
μ_2	$4\pi \times 10^{-7}(\text{H/m})$	Permeability of the Surrounding Space

the radiation pattern $F_n(\phi)$ will not contribute divergent behavior, so long as the product of remaining terms converge.

We will make extensive use of the ratio test (41), which states that a series $\sum \alpha_n$ converges if

$$\limsup_{n \rightarrow \infty} \left| \frac{\alpha_{n+1}}{\alpha_n} \right| < 1. \quad (4.13)$$

The ratio test implicitly tests for the property that, for convergence, we must have

$$\limsup_{n \rightarrow \infty} \alpha_n = 0 \quad (4.14)$$

which is a necessary, but not sufficient, condition for convergence. Thus the ratio test provides a strong test of convergence, and we see that we will need to evaluate the expression

$$\limsup_{n \rightarrow \infty} \left| \frac{a_{n+1} p_{n+1}}{a_n p_n} \right| \quad (4.15)$$

in order to understand the behavior of the sum. Again, we can evaluate this in a piecewise manner. First, we evaluate the p_n contribution

$$\limsup_{n \rightarrow \infty} \left| \frac{p_{n+1}}{p_n} \right| \quad (4.16)$$

$$\limsup_{n \rightarrow \infty} \left| \frac{\left(\frac{1}{\sin \frac{\phi_0}{2}} \frac{(-i \cot \frac{\phi_0}{2})^{n+1}}{(n+1)!} \right)}{\left(\frac{1}{\sin \frac{\phi_0}{2}} \frac{(-i \cot \frac{\phi_0}{2})^n}{n!} \right)} \right| \quad (4.17)$$

$$\boxed{\limsup_{n \rightarrow \infty} \left| \frac{(-i \cot \frac{\phi_0}{2})}{(n+1)} \right| = 0.} \quad (4.18)$$

This limit follows from our earlier restriction of the domain of $\frac{\pi}{2} \leq \phi_0 \leq \pi$ and thus the range of $\cot \frac{\phi_0}{2}$ is $(1, 0)$ over this domain. We are off to a good start for showing that the series converges.

Now we consider the more difficult limit

$$\limsup_{n \rightarrow \infty} \left| \frac{a_{n+1}}{a_n} \right| \quad (4.19)$$

Let's first restate Equation 2.27

$$a_n = \frac{1}{D_{-n-1}(\eta_2 \gamma^+)} c_n \left(D_{-n-1}(\eta_2 \gamma^+) - \frac{D_{-n-1}(\eta_1 \gamma^+)}{D_n(\eta_1 \gamma^-)} D_n(\eta_2 \gamma^-) \right) - \frac{D_n(\eta_2 \gamma^-)}{D_{-n-1}(\eta_2 \gamma^+)}$$

which we can rearrange as

$$a_n = c_n \left(1 - \frac{D_{-n-1}(\eta_1 \gamma^+) D_n(\eta_2 \gamma^-)}{D_n(\eta_1 \gamma^-) D_{-n-1}(\eta_2 \gamma^+)} \right) - \frac{D_n(\eta_2 \gamma^-)}{D_{-n-1}(\eta_2 \gamma^+)} \quad (4.20)$$

and notice that the behavior of these coefficients will be dependent upon the behavior of $D_n(\zeta)$ and $D_{-n-1}(\zeta)$ as $n \rightarrow \infty$. Our first step will be find an expression for $D_n(\zeta)$ and $D_{-n-1}(\zeta)$ for large n , and let's use the dummy variable β to describe the behavior of each of these as such. That is, we can think of each function as $D_\beta(\zeta)$. Our series is only over positive, increasing values of n . For $\beta = n$, this corresponds to increasing values of β , but for $\beta = -n - 1$, this corresponds to decreasing values of β . Thus we must find expressions for $D_\beta(\zeta)$ for $\beta \rightarrow \pm\infty$.

For $\beta \rightarrow \infty$, we found in Equation 1.27 that $D_\beta(\zeta)$ takes the form

$$D_\beta(\zeta) = e^{-\zeta^2/4} 2^{-\beta/2} H_\beta(2^{-1/2} \zeta)$$

where again the H_β is the Hermite polynomial of degree β . At this point it is helpful to talk a bit more about the Hermite polynomials. These polynomials are recursively defined, and from (40)

$$H_\beta(\zeta) = \sum_{m=0}^{\beta} k_m \zeta^m \quad (4.21)$$

where the k_m are normalization coefficients, and any term with opposite parity to β has $k_m = 0$. The calculation of these coefficients is inconsequential to this thesis, however the general form of the equation is of importance in our calculations. An example of a Hermite polynomial for $\beta = 6$ is

$$H_6(\zeta) = 64\zeta^6 - 480\zeta^4 + 720\zeta^2 - 120. \quad (4.22)$$

To bring this back to our discussion of the analysis of the Hermite polynomial as $\beta \rightarrow \infty$, we see that to leading order, we can simply express the polynomial as

$$H_\beta(\zeta) = (2\zeta)^\beta. \quad (4.23)$$

Pulling this back into our expression for the parabolic cylinder function in the limit of large β , we replace β with n and we find

$$D_n(\zeta) = e^{-\zeta^2/4} \zeta^n \quad (4.24)$$

which we will use moving forward

In the limit $\beta \rightarrow -\infty$, which corresponds to $\beta = -n - 1$, we have to leading order

$$D_{-n-1}(\zeta) = \frac{\sqrt{\pi}}{(2^{(n+1)/2})\Gamma(1 + \frac{n}{2})} e^{-\zeta\sqrt{n+\frac{1}{2}}} \quad (4.25)$$

which is given in (40). For the first time, we make use of the gamma function, represented in the equation by Γ . We will do our best to refrain from diving too deeply into the properties of the Γ function, simply put, it is the analytic continuation of the factorial function (42). Specifically, for integer arguments, $\Gamma(n) = (n-1)!$. In our case, we will be more interested in half-integer arguments, which are expressed by

$$\Gamma(n/2) = \frac{(n-2)!!\sqrt{\pi}}{2^{(n-1)/2}}. \quad (4.26)$$

This is far from an exhaustive treatment of the Γ function, but for now let's return to our parabolic cylinder function expressions. We insert our new expressions for $D_n(\zeta)$ and $D_{-n-1}(\zeta)$ into Equation 4.20, specifically the fraction inside the parenthesis.

$$\left(\frac{D_{-n-1}(\eta_1 \gamma^+) D_n(\eta_2 \gamma^-)}{D_n(\eta_1 \gamma^-) D_{-n-1}(\eta_2 \gamma^+)} \right) \quad (4.27)$$

$$= \frac{\frac{\sqrt{\pi}}{(2^{(n+1)/2})\Gamma(1 + \frac{n}{2})} \exp \left[-(\eta_1 \gamma^+) \sqrt{n + \frac{1}{2}} - (\eta_2 \gamma^-)^2/4 \right] (\eta_2 \gamma^-)^n}{\frac{\sqrt{\pi}}{(2^{(n+1)/2})\Gamma(1 + \frac{n}{2})} \exp \left[-(\eta_2 \gamma^+) \sqrt{n + \frac{1}{2}} - (\eta_1 \gamma^-)^2/4 \right] (\eta_1 \gamma^-)^n} \quad (4.28)$$

$$= \frac{\exp \left[-(\eta_1 \gamma^+) \sqrt{n + \frac{1}{2}} - (\eta_2 \gamma^-)^2/4 \right] (\eta_2 \gamma^-)^n}{\exp \left[-(\eta_2 \gamma^+) \sqrt{n + \frac{1}{2}} - (\eta_1 \gamma^-)^2/4 \right] (\eta_1 \gamma^-)^n} \quad (4.29)$$

$$= \exp \left[\sqrt{n + \frac{1}{2}} \gamma^+ (\eta_2 - \eta_1) - \gamma^{-2} (\eta_2^2 - \eta_1^2)/4 \right] \left(\frac{\eta_2}{\eta_1} \right)^n. \quad (4.30)$$

The reader will note here that we have begun to use the notation $\exp(x) \equiv e^x$ for clarity as many of our exponential terms are becoming clumsy. Evaluating this term to the limit $n \rightarrow \infty$ yields

$$= \exp \left[\sqrt{n} \gamma^+ (\eta_2 - \eta_1) \right] \left(\frac{\eta_2}{\eta_1} \right)^n. \quad (4.31)$$

Following the same approach, we evaluate the last term in Equation 4.20 by way of

$$\frac{D_n(\eta_2\gamma^-)}{D_{-n-1}(\eta_2\gamma^+)} = \frac{e^{-(\eta_2\gamma^-)^2/4}(\eta_2\gamma^-)^n}{\left(\frac{\sqrt{\pi}}{(2^{(n+1)/2})\Gamma(1 + \frac{n}{2})}e^{-(\eta_2\gamma^+)\sqrt{n+\frac{1}{2}}}\right)} \quad (4.32)$$

which can be rearranged as

$$= \frac{\exp\left((\eta_2\gamma^+)\sqrt{n+\frac{1}{2}} - (\eta_2\gamma^-)^2/4\right)(\eta_2\gamma^-)^n(2^{(n+1)/2})\Gamma(1 + \frac{n}{2})}{\sqrt{\pi}}. \quad (4.33)$$

Again, we can significantly simplify this expression by evaluating it in the limit $n \rightarrow \infty$

$$= \frac{\Gamma(\frac{n}{2}) \exp(\sqrt{n}(\eta_2\gamma^+))(\sqrt{2}\eta_2\gamma^-)^n}{\sqrt{\pi}}. \quad (4.34)$$

We have specifically chosen to place the Γ function as the first term in the numerator, since its behavior with increasing n will dominate the entire expression. For example, we can see that the Γ function grows even faster than the exponential function with increasing argument

$$\lim_{n \rightarrow \infty} \frac{\Gamma(n)}{e^n} = \infty, \quad (4.35)$$

Let's now address the coefficient c_n . Recall from Equation 2.29 that we calculate c_n as

$$\begin{aligned} c_n = & Y_2 \left[iD'_n(\eta_2\gamma^-) + \frac{D_n(\eta_2\gamma^-)}{D_{-n-1}(\eta_2\gamma^+)} D'_{-n-1}(\eta_2\gamma^+) \right] \\ & \times \left[Y_2 \frac{D'_{-n-1}(\eta_2\gamma^+)}{D_{-n-1}(\eta_2\gamma^+)} \left(D_{-n-1}(\eta_2\gamma^+) - \frac{D_{-n-1}(\eta_1\gamma^+)}{D_n(\eta_1\gamma^-)} D_n(\eta_2\gamma^-) \right) \right. \\ & \left. - iY_1 \frac{D_{-n-1}(\eta_1\gamma^+)}{D_n(\eta_1\gamma^-)} D'_n(\eta_2\gamma^-) - Y_1 D'_{-n-1}(\eta_2\gamma^+) \right]^{-1}. \end{aligned}$$

We see that we need expressions for the derivatives of the parabolic cylinder functions we just described. Immediately applying the simplification found from taking the limit $n \rightarrow \infty$ and using dummy constant k for evaluating the derivatives, we find

$$D'_n(k\zeta) = n\zeta^{(n-1)} \exp(-(k\zeta)^2/4) \quad (4.36)$$

$$D'_{-n-1}(k\zeta) = \frac{k\sqrt{\pi(n+\frac{1}{2})}}{(2^{(n+1)/2})\Gamma(1+\frac{n}{2})} e^{-k\zeta\sqrt{n+\frac{1}{2}}}. \quad (4.37)$$

We wish to insert these values into c_n to observe its behavior with increasing n , but a quick inspection of Equation 2.29 hints that this expression will not lend itself to clarity. Let us

then make the following substitutions for the parabolic cylinder functions and their derivatives, omitting any constants and assuming all arguments to be equal to κ ,

$$D_n(\kappa) \sim \kappa^n \quad (4.38)$$

$$D'_n(\kappa) \sim n\kappa^{(n-1)} \quad (4.39)$$

$$D_{-n-1}(\kappa) \sim \frac{\exp(\sqrt{n})}{\Gamma(\frac{n}{2})2^{n/2}} \quad (4.40)$$

$$D'_{-n-1}(\kappa) \sim \frac{\sqrt{n} \exp(\sqrt{n})}{\Gamma(\frac{n}{2})2^{n/2}}. \quad (4.41)$$

Utilizing these expressions in Equation 2.29, we find

$$c_n \sim \left[n\kappa^{(n-1)} + \sqrt{n}\kappa^n \right] \times \left[\frac{\exp(\sqrt{n})}{\Gamma(\frac{n}{2})2^{n/2}} \left(\sqrt{n} \left(1 - \frac{\kappa^n}{\kappa^n} \right) + n + \sqrt{n} \right) \right]^{-1}. \quad (4.42)$$

Again, this can be further simplified by taking the limit $n \rightarrow \infty$,

$$c_n \sim \frac{n\kappa^{(n-1)}}{\left(\frac{n \exp(\sqrt{n})}{\Gamma(\frac{n}{2})2^{n/2}} \right)} \quad (4.43)$$

$$c_n \sim \frac{\Gamma(\frac{n}{2})2^{n/2}\kappa^{(n-1)}}{\exp(\sqrt{n})} \quad (4.44)$$

In a similar fashion, we rewrite Equation 4.31 and Equation 4.34 as

$$\exp \left[\sqrt{n} \gamma^+ (\eta_2 - \eta_1) \right] \left(\frac{\eta_2}{\eta_1} \right)^n \sim \exp (\sqrt{n}) \kappa^n \quad (4.45)$$

$$\frac{\Gamma(\frac{n}{2}) \exp (\sqrt{n} (\eta_2 \gamma^+)) (\sqrt{2} \eta_2 \gamma^-)^n}{\sqrt{\pi}} \sim \Gamma(\frac{n}{2}) \exp (\sqrt{n}) \kappa^n \quad (4.46)$$

where constants have been replaced by and inserting these expressions, along with Equation 4.44 into Equation 4.20 yields

$$a_n \sim \frac{\Gamma(\frac{n}{2}) 2^{n/2} \kappa^{(n-1)}}{\exp (\sqrt{n})} \left(1 - \exp (\sqrt{n}) \kappa^n \right) - \Gamma(\frac{n}{2}) \exp (\sqrt{n}) \kappa^n. \quad (4.47)$$

We notice that the form of both parts of the right-hand side take a similar form, and upon recognizing that constant factors have been omitted as it is only the gross behavior of the expression that we are interested in, we again apply the limit $n \rightarrow \infty$ and simplify the expression to

$$\boxed{a_n \sim \Gamma(\frac{n}{2}) \kappa^{(n)}} \quad (4.48)$$

Now, we finally have everything we need to directly test the convergence of our series, i.e. to calculate the result of Equation 4.15. Recall we calculated the \mathbf{p}_n component in Equation 4.18, and now we can calculate the expression first stated in Equation 4.19,

$$\boxed{\limsup_{n \rightarrow \infty} \left| \frac{\mathbf{a}_{n+1}}{\mathbf{a}_n} \right| = \limsup_{n \rightarrow \infty} \left| \frac{\Gamma(\frac{n+1}{2}) \kappa^{(n+1)}}{\Gamma(\frac{n}{2}) \kappa^{(n)}} \right| = \limsup_{n \rightarrow \infty} \left| \frac{\Gamma(\frac{n+1}{2}) \kappa}{\Gamma(\frac{n}{2})} \right| = \limsup_{n \rightarrow \infty} \left| \sqrt{\frac{n}{2}} \kappa \right|.} \quad (4.49)$$

Where we have use the expression for the ratio of gamma functions given as (43)

$$\text{If } n \rightarrow \infty \text{ then } \frac{\Gamma(n + \alpha)}{\Gamma(n + \beta)} \sim n^{\alpha - \beta} \quad (4.50)$$

Let us use this result, along with the result of Equation 4.18 in Equation 4.15

$$\boxed{\limsup_{n \rightarrow \infty} \left| \frac{\mathbf{a}_{n+1} \mathbf{p}_{n+1}}{\mathbf{a}_n \mathbf{p}_n} \right| = \limsup_{n \rightarrow \infty} \left| \frac{\sqrt{\frac{\pi}{2}} \kappa (-i \cot \frac{\phi_0}{2})}{(n+1)} \right| = 0} \quad (4.51)$$

and since this limit is less than one, we see that our series is convergent. As a sanity check, we can see also verify that the condition specified in Equation 4.14 is fulfilled,

$$\limsup_{n \rightarrow \infty} \mathbf{a}_n \mathbf{p}_n = \limsup_{n \rightarrow \infty} \frac{\Gamma(\frac{n}{2}) \kappa^n (-i \cot \frac{\phi_0}{2})^n}{\sin \frac{\phi_0}{2} n!} = 0. \quad (4.52)$$

Thus, we have shown that the series expansion for our scattered fields will *always* converge over the domain of the problem; a superb result.

4.6 The Scattered Field

Finally, we have everything we need to plot and observe the scattered field of our problem geometry. All plots presented in this section were produced utilizing the variable values defined in Table I. The field is plotted for the sum up to a value of n indicated in the legend of each figure to demonstrate the convergence of the infinite sums. The plotted fields are intentionally left unnormalized so that the reader may get a better sense of the relative strength of the scattered field in each plot.

Consider the simplest case, the scattered field from a plane wave incident from the negative x -axis, i.e. $\phi_0 = \pi$. This case is presented Figure 15, where we have plotted the magnitude of the total field. We see the 0th order shape of the radiation pattern which we derived in Equation 4.10, and it is apparent that only the $n = 0$ term contributes to the scattered field, as expected. In Figure 16, we have plotted the phase angle of the complex field as a function of scattering angle ϕ , and we notice that the phase of the scattered field is constant. These two plots may not be visually stimulating, however they provide a baseline for comparison with the plots we shall soon see.

Far-Field Scattering by an Isorefractive Parabolic Sheath
 $|\Psi_s(\phi)|$, $\phi_0: 180^\circ$

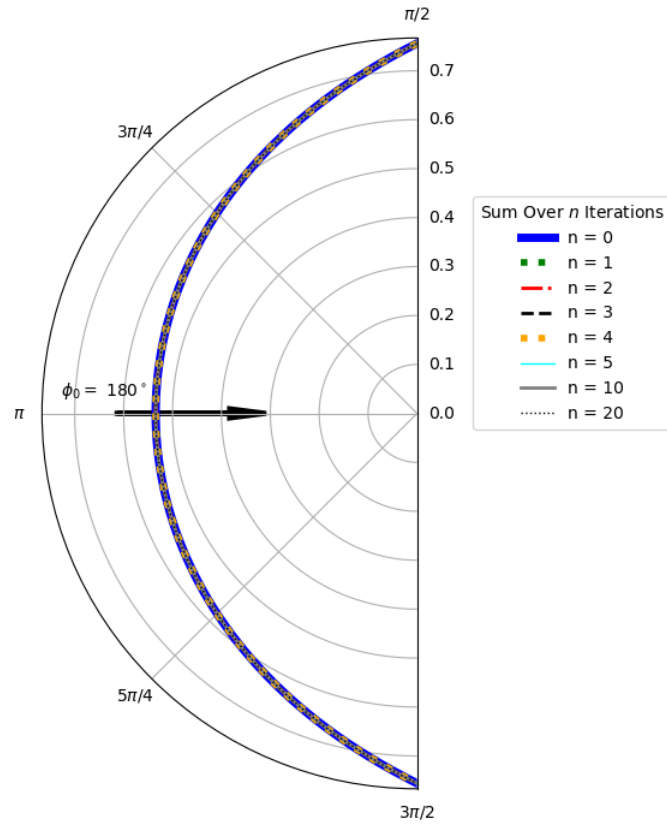


Figure 15: Far-field scattering, $|\Psi_s(\phi)|$, $\phi_0 = \pi$

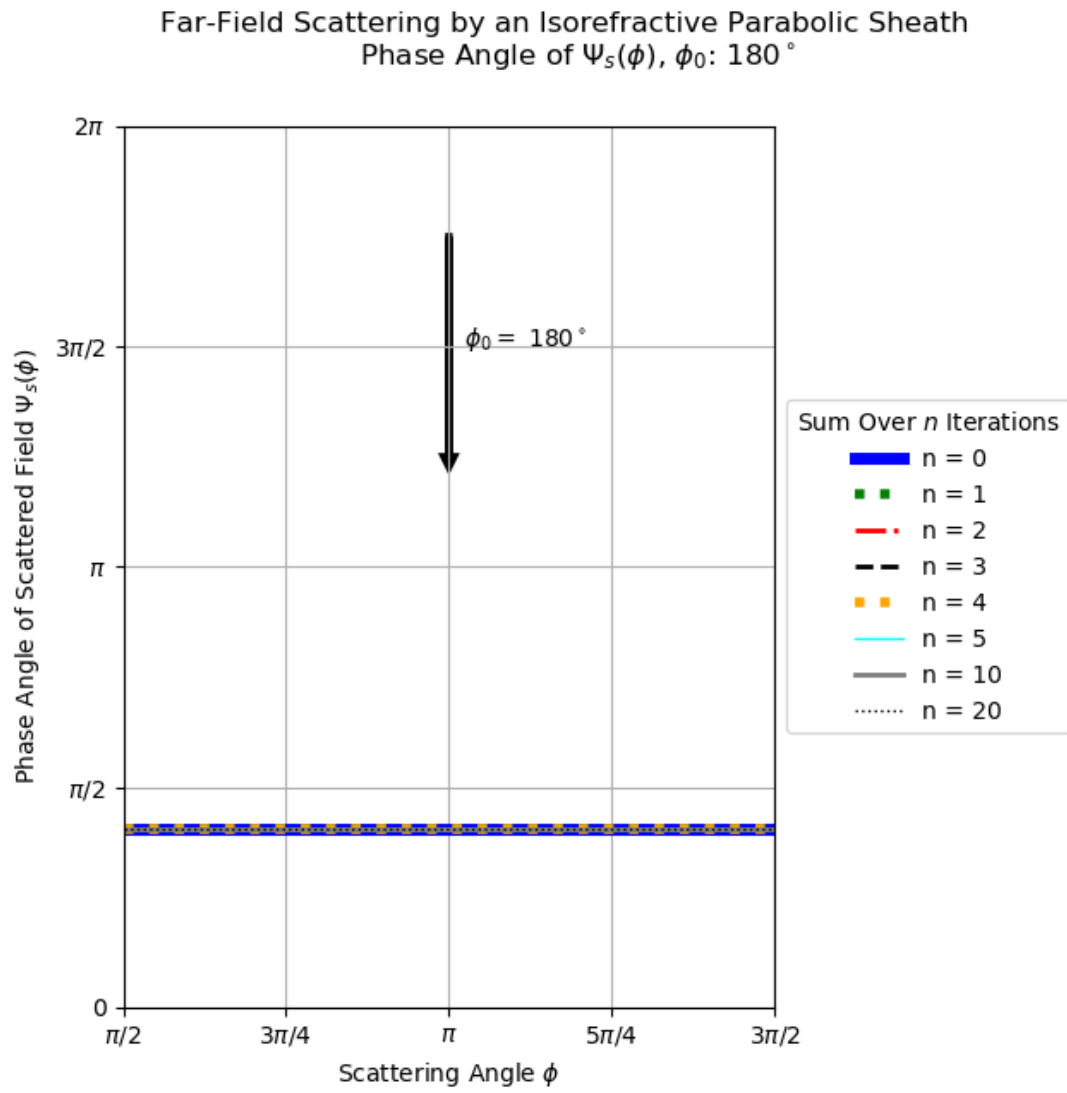


Figure 16: Far-field scattering phase angle of $\Psi_s(\phi)$, $\phi_0 = \pi$

Figure 17 modifies the setup of Figure 15 slightly by changing the angle of incidence by 10 degrees, i.e. $\phi_0 = \frac{17\pi}{18} = 170^\circ$. Notice here that higher order contributions of the sum shift the scattered field away from the symmetric radiation pattern we saw in Figure 15, as expected. In particular, we see that the scattered field is stronger in the $+\mathbf{y}$ direction, due to the parabolic cylinders reflecting the incident wave back towards the angle of incidence. Because ϕ_0 is still relatively close to the x-axis, the series converges quickly. Figure 18 shows the phase angle of the scattered field for this angle of incidence, and we see that the impact on the phase of the scattered field as a function of ϕ is such that the phase is no longer constant, although only slightly so, and most notably along the \mathbf{y} -axis.

Far-Field Scattering by an Isorefractive Parabolic Sheath
 $|\Psi_s(\phi)|$, $\phi_0: 170^\circ$

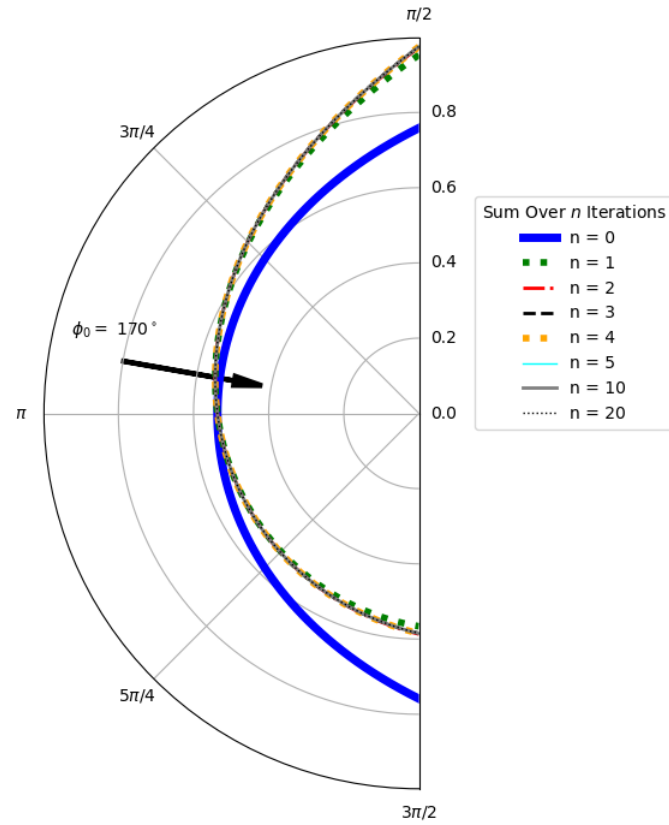


Figure 17: Far-field scattering, $|\Psi_s(\phi)|$, $\phi_0 = \frac{17\pi}{18}$

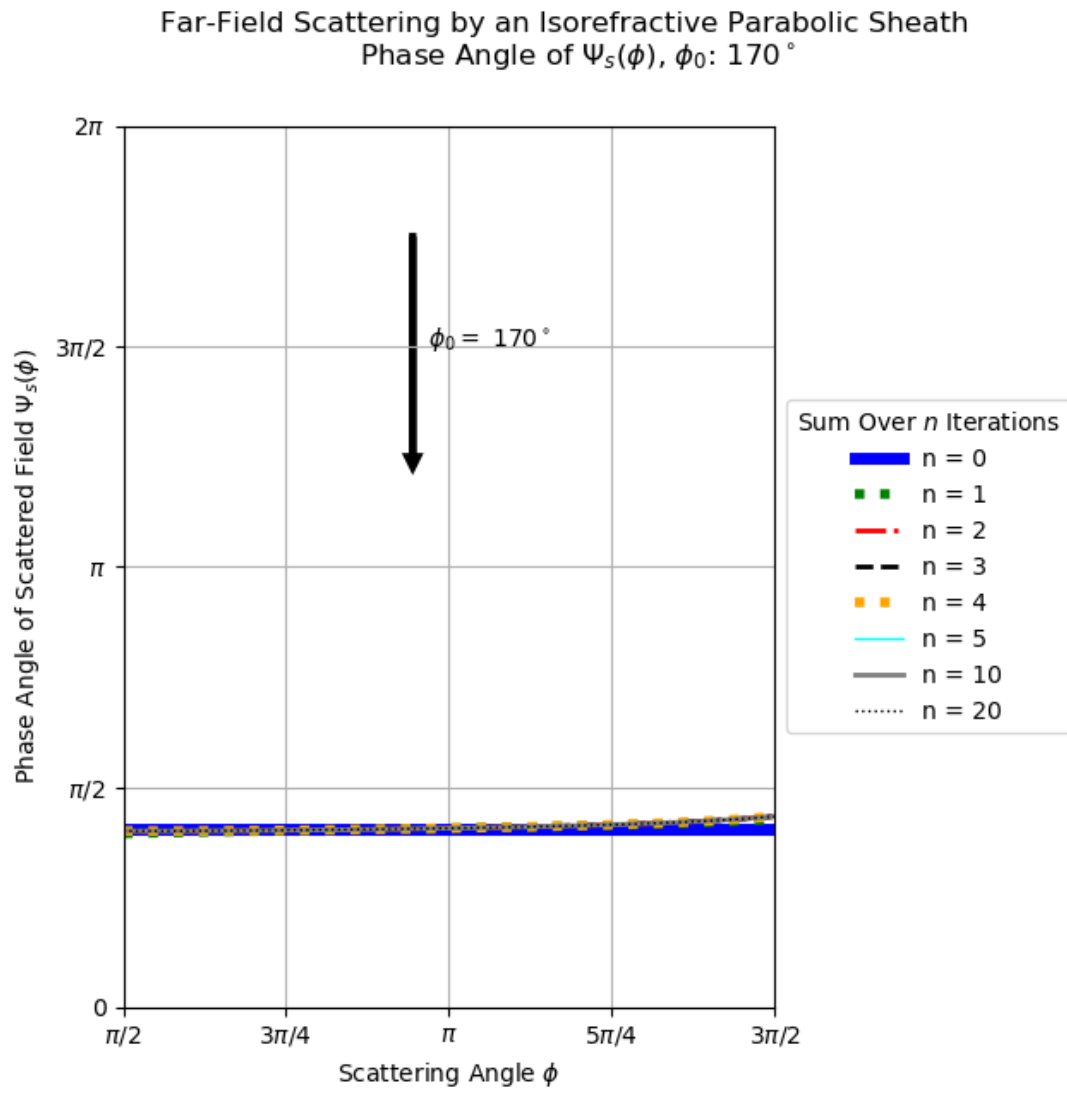


Figure 18: Far-field scattering phase angle of $\Psi_s(\phi)$, $\phi_0 = \frac{17\pi}{18}$

If we move the angle of incidence further from the x-axis, we start to see even more interesting behavior, as in Figure 19. Here, we have shifted the angle of incidence more substantially to $\phi_0 = \frac{3\pi}{4} = 135^\circ$. The series converges more slowly than in the previous plots, and as we saw in Figure 17, the scattered field is stronger reflecting back in the direction of the incident wave. Figure 20 again plots the phase of the scattered field, and we see that the phase angle is more varied across the scattering angles, and that the field sum converges more slowly than in previous setups. If the incident wave is reflected about the x-axis ($\phi_0 = \frac{5\pi}{4}$), we produce mirror image plots (Figure 21, Figure 22), as expected.

Far-Field Scattering by an Isorefractive Parabolic Sheath
 $|\Psi_s(\phi)|$, $\phi_0: 135^\circ$

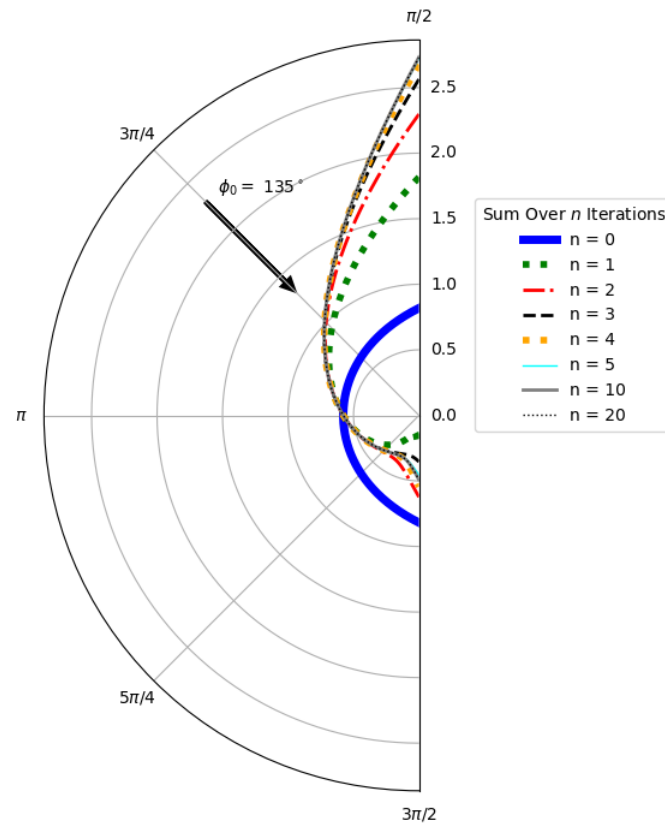


Figure 19: Far-field scattering, $|\Psi_s(\phi)|$, $\phi_0 = \frac{3\pi}{4}$

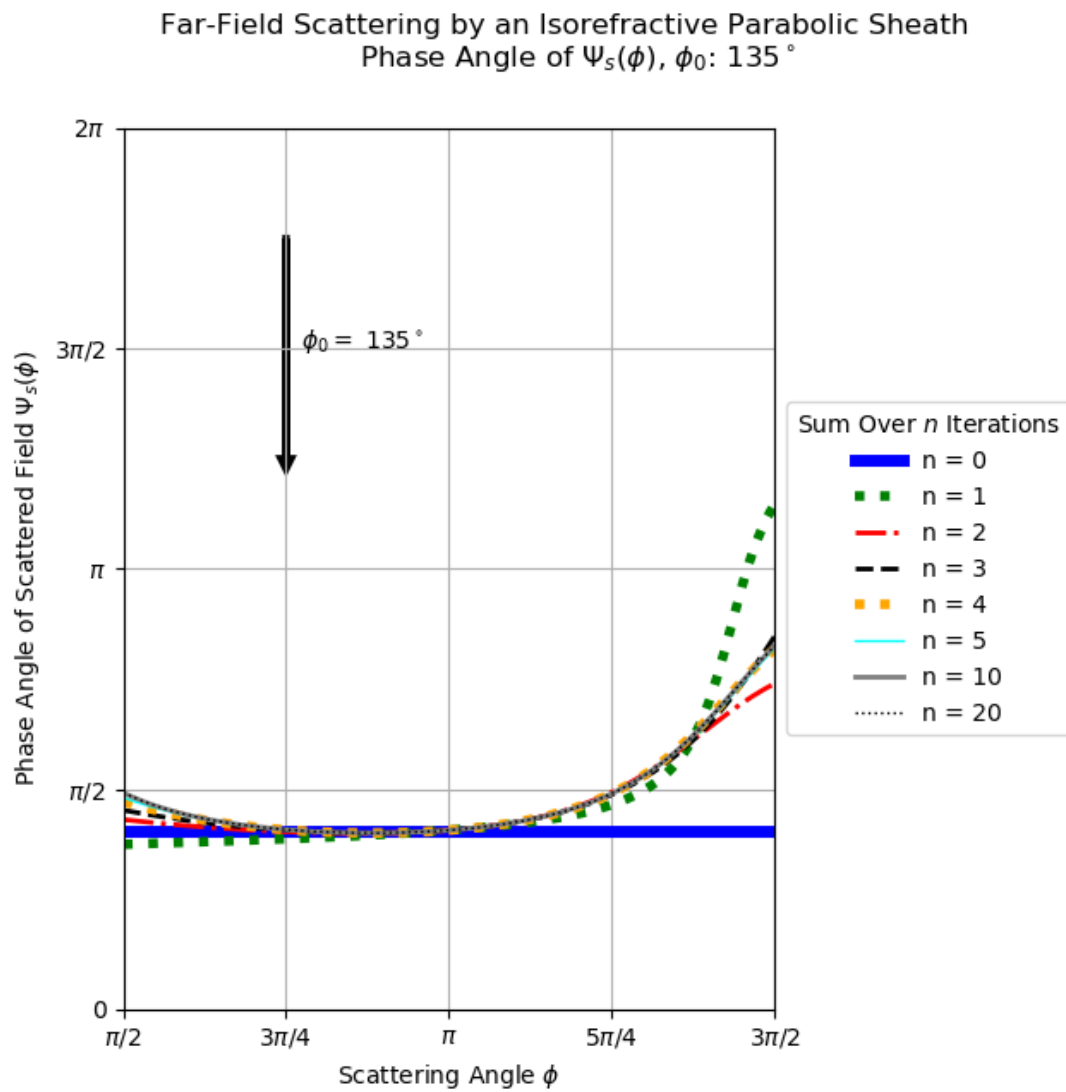


Figure 20: Far-field scattering phase angle of $\Psi_s(\phi)$, $\phi_0 = \frac{3\pi}{4}$

Far-Field Scattering by an Isorefractive Parabolic Sheath
 $|\Psi_s(\phi)|$, $\phi_0: 225^\circ$

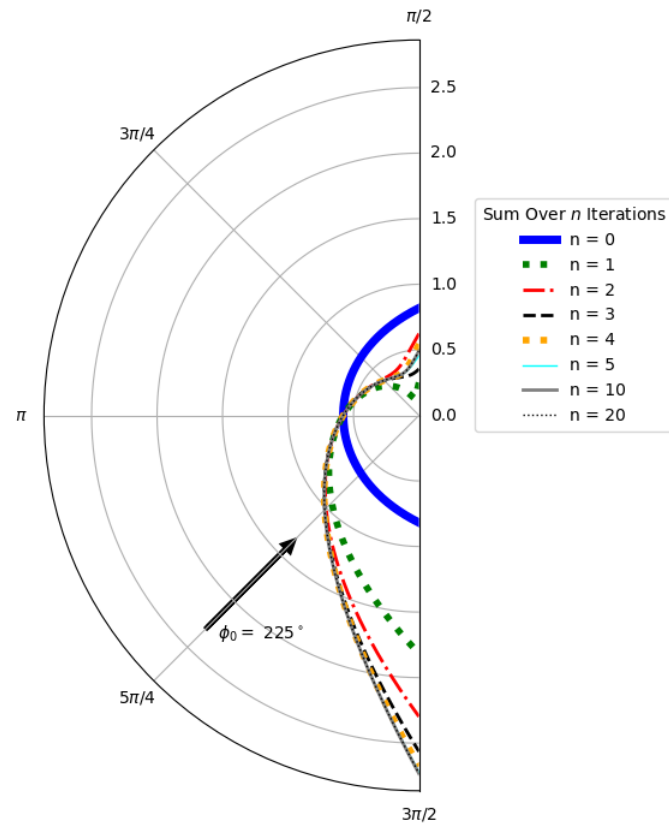


Figure 21: Far-field scattering, $|\Psi_s(\phi)|$, $\phi_0 = \frac{5\pi}{4}$

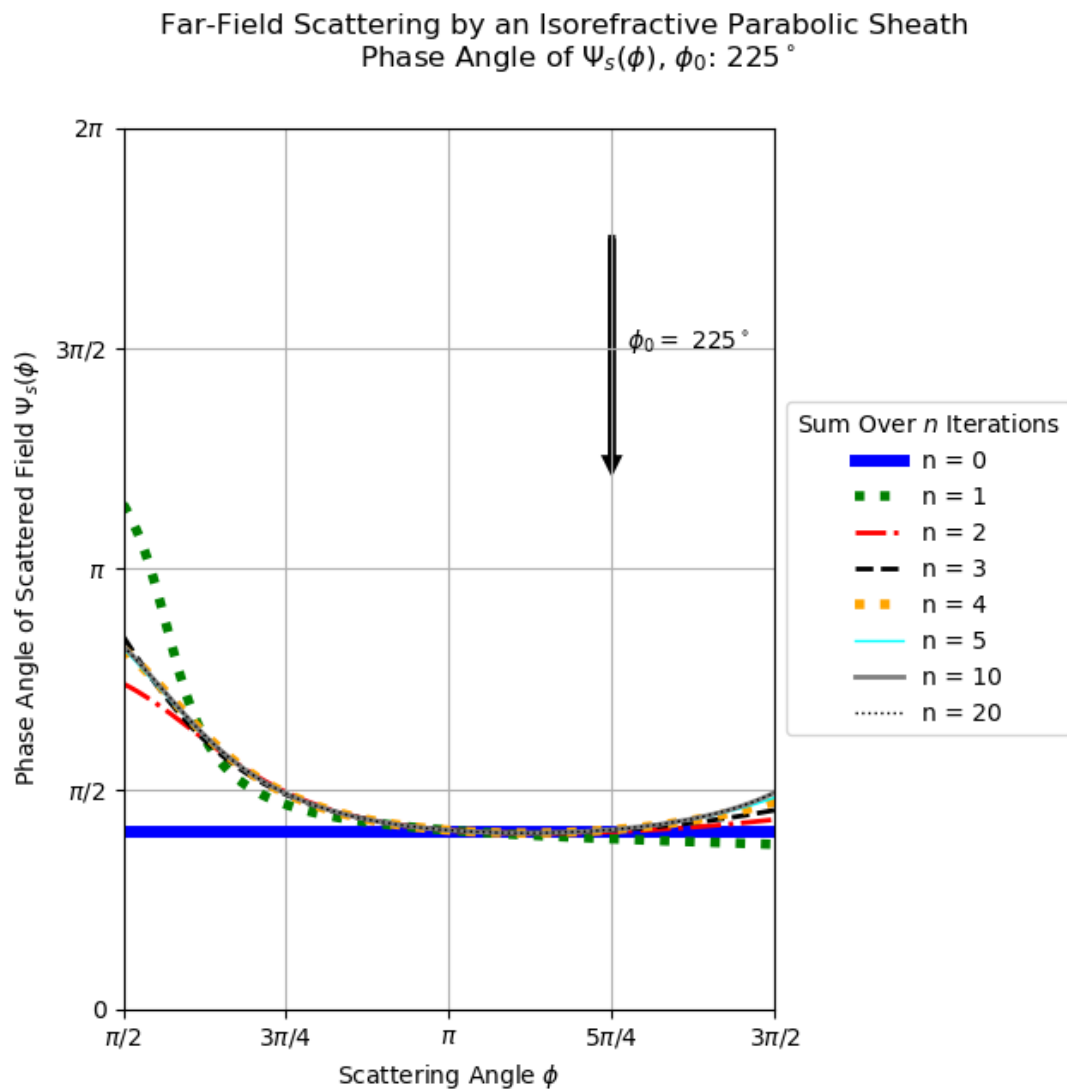


Figure 22: Far-field scattering phase angle of $\Psi_s(\phi)$, $\phi_0 = \frac{5\pi}{4}$

If the incident wave is moved to an even more extreme angle, here $\phi_0 = \frac{11\pi}{18} = 110^\circ$, we observe more exaggerated behavior, as seen in Figure 23 and Figure 24. We see that very little of the field is scattered into the $-\mathfrak{y}$ region. In these plots, along the \mathfrak{y} -axis, even summing over twenty terms of \mathfrak{n} we do not see the sum converging quickly. Additionally, we see significant variation of the phase angle across the scattered field.

Far-Field Scattering by an Isorefractive Parabolic Sheath
 $|\Psi_s(\phi)|$, $\phi_0: 110^\circ$

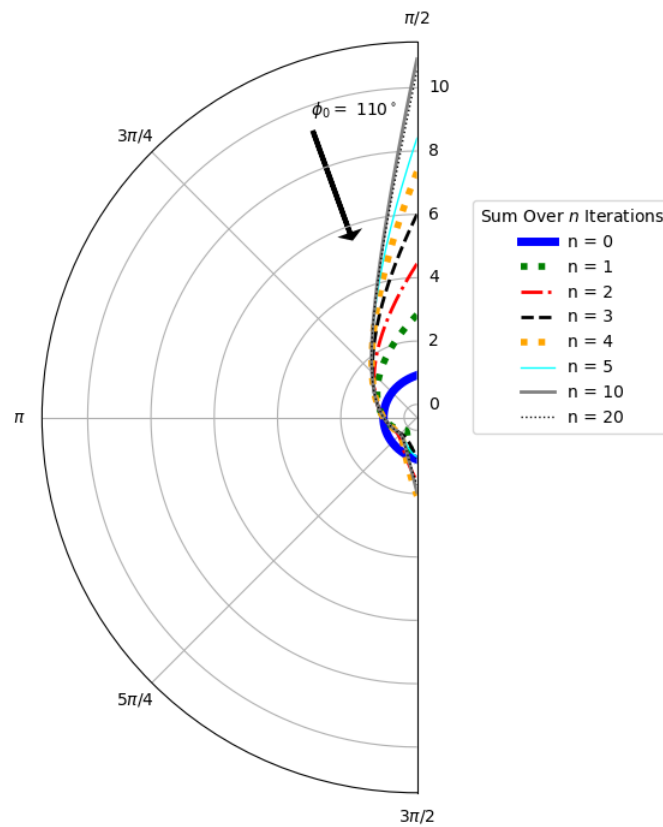


Figure 23: Far-field scattering, $|\Psi_s(\phi)|$, $\phi_0 = \frac{11\pi}{18}$

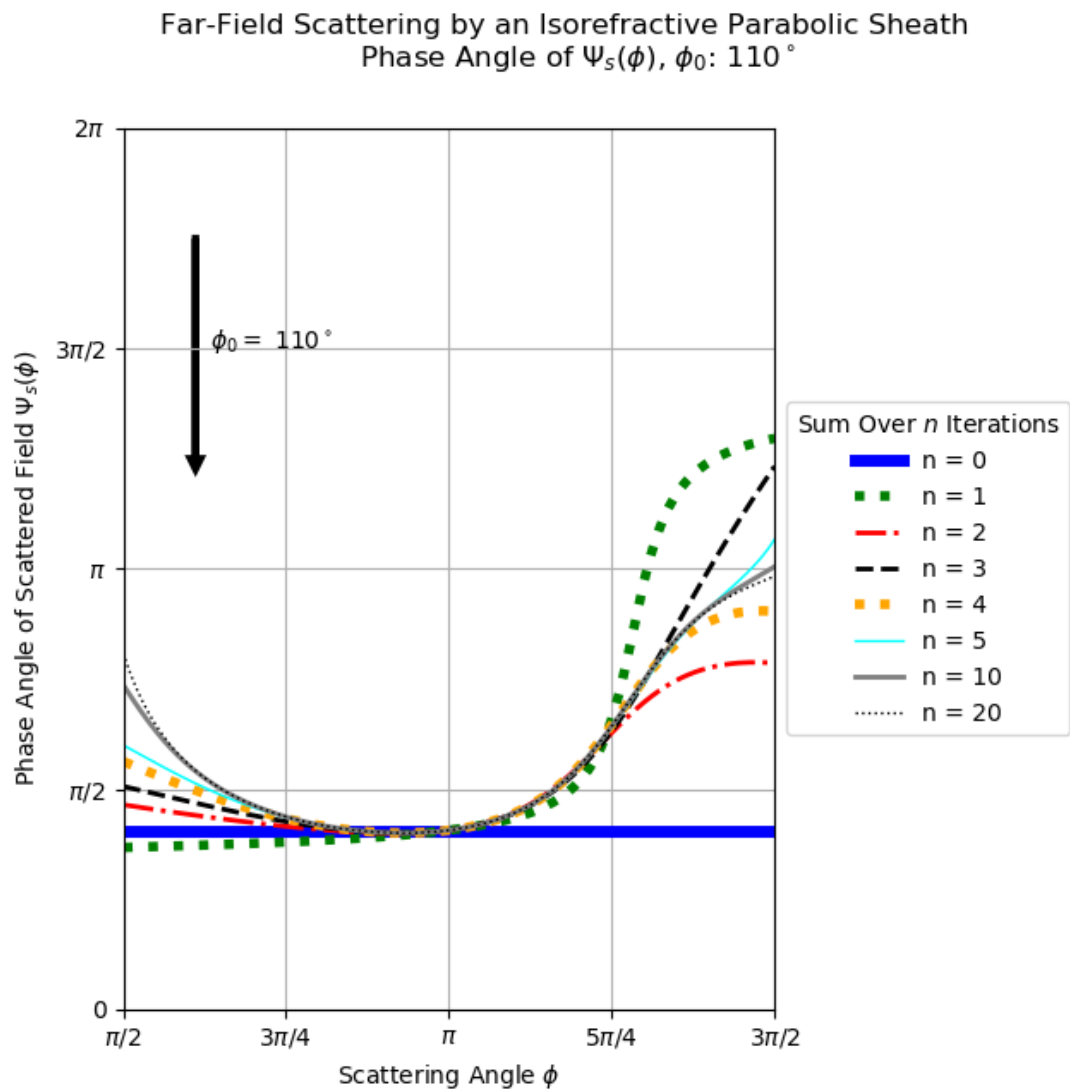


Figure 24: Far-field scattering phase angle of $\Psi_s(\phi)$, $\phi_0 = \frac{11\pi}{18}$

Thus, we see that our analysis over the previous sections has allowed us to visualize and analyze the scattered fields produced in our problem geometry. With the tools we have developed, there is a wide range parameters we can vary and behaviors we can explore.

4.7 Software

Before moving on, we will take a moment to discuss the software used in calculating our solutions. All calculations and plots were produced using Python 3.6. A number of libraries were used extensively, especially Matplotlib, NumPy, and SymPy. Most importantly, calculation of the PCF and their derivatives was accomplished with the mpmath library. mpmath allows for arbitrary precision of calculation, and is cited by the “Digital Library of Mathematical Functions” for implementation of these functions in Python. Samples of the authors code which was used to calculate and plot the scattered fields, as well as a useful python library of related functions, are provided in the appendix.

CHAPTER 5

CONCLUDING REMARKS

Finally, we have reached the end of our journey, and it would do well to recap all that we have covered. We started by taking a deep-dive into the parabolic cylinder coordinate system, and covered the mathematical relations necessary for us in this geometry. We presented novel analytic results for the problem of a plane wave scattering from a PEC parabolic cylinder embedded in a confocal isorefractive material for incident waves with both electric and magnetic polarizations. We dove deeply into the numerical behavior of our problem geometry, deriving expressions for the far-field asymptotic scattering, assessing the convergence behavior of our infinite sums, and generating plots of the scattered field. Thus, a new exact canonical solution of an electromagnetic scattering problem has been found.

The utility of the results presented herein should be clear: we now have an exact analytic solution for a relatively complex and useful geometry which can be used as a benchmark in evaluating the performance of computational software (5). One can simulate our problem geometry in an electromagnetic modeling program and evaluate the accuracy of the results using the expressions, methods and tools developed in this thesis. Our geometry is a useful example because it can be used to approximate many real-world objects, such as the wing of an airplane, or the hood of a car.

A geometry such as ours presents a rich problem space to study, one which would provide an intrepid researcher plenty of opportunity to explore and discover even more interesting results.

There are many ways that this analysis can be applied to similar problems and geometries as well; this field of study is rich with fascinating problems. However, for the time being, I leave these results for anyone who may make good use of them, with the hope that an interesting application in need of these tools will arise.

APPENDIX

A.1 Parabolic Cylinder Function Library

The python library below was written in support of this thesis. It forms a library of functions which may be useful when working in a parabolic cylinder geometry, and was made use of extensively in developing and writing this thesis. The code was written for python 3.6, and makes use of additional external libraries.

For reference, this library was saved as “pcf_lib”, and is imported into the scripts in A.2 and A.3 under this name.

```

### PCF Library

# This library will contain all the parabolic cylinder
# functions we'll need moving forward

from math import sqrt, factorial

import mpmath as mp

from mpmath import erf, exp, pcfd, diff, pi, cos, sin, tan

import sympy as sp

from numpy import array, sort, column_stack

import pandas as pd

```

APPENDIX (Continued)

```

# mpmath settings

mp.dps = 25

mp.pretty = True

def cart2pc(x, y):
    # Convert from cartesian (x, y) to parabolic cylinder coordinates (eta,
↪ xi)

    if (y == 0) and (x <= 0):
        xi = 0
        eta = sqrt(-2*x)
    else:
        eta_2 = (y ** 2) / (x + sqrt(x ** 2 + y ** 2))
        xi_2 = x + sqrt(x ** 2 + y ** 2)
        eta = sqrt(eta_2)

        if y >= 0:
            xi = sqrt(xi_2)

        elif y < 0:
            xi = - sqrt(xi_2)

```

APPENDIX (Continued)

```

        else:

            return False

    pc_crd = [eta, xi]

    return pc_crd

def dndzexp(n, z):

    # calculate the nth derivative of exp(z**2 / 2), to be used in

    # pcf_d_n_minus_1

    x = sp.Symbol('x')

    f = sp.exp((x ** 2) / 2)

    for i in range(0, n):

        f = sp.Derivative(f, x)

    h = f.doit()

    sum_total = h.evalf(subs={x: z})

    return sum_total

def dndz_exp_erf(n, z):

    # calculate the nth derivative of exp(z**2 / 2) * erf(z/sqrt(2)),

```

APPENDIX (Continued)

```

# to be used in pcfd_n_minus_1

x = sp.Symbol('x')

f = sp.exp((x**2)/2) * sp.erf(x/mp.sqrt(2))

for i in range(0, n):

    f = sp.Derivative(f, x)

h = f.doit()

sum_total = h.evalf(subs={x: z})

return sum_total


def dndzerf_old(n, z):

    # Calculate the nth derivative of the error function erf, to be used in
    # pcfd_n_minus_1 Update since adding _old suffix, this has been replaced
    # by both dndzerf and dndz_exp_erf

    m = n-1

    sum_total = ((-1)**m) * (2/mp.sqrt(mp.pi)) * mp.hermite(m, z) *
    ↪ mp.exp(-(z**2))

    return sum_total


def pcfd_n_minus_1(n, z):

```

APPENDIX (Continued)

```

# Calculate the value of  $D_{\{-n-1\}}(z)$ 

if n == 0:

    value = sqrt(2) * exp(-(z**2)/4) * (exp((z**2)/2) - (exp((z**2)/2) *
                                                    erf(z/sqrt(2))))

else:

    value = sqrt(2) * (((-1)**n)/factorial(n)) * exp(-(z**2)/4) * (
        dndzexp(n, z) - dndz_exp_erf(n, z))

return value

def pcdf_prime(n, z, a):

    # Calculate the derivative of the pcdf function.

    # Special note that this function will divide out the factor of a from
    # the numerator before returning the value, because of the math we did in
    # representing the function n is the order of the polynomial z is the
    # argument with respect to differentiation a is a constant multiplying dx
    # is the order of differentitaion (1 = first derivative, etc...) This is
    # now being update to use the mpmath derivative, instead of symbolic
    ↪ math

    # Looking at the function: x will be eta or xi

    # a is the 'gamma' constane ( $\text{Exp}(i \pi / 4) * \text{sqrt}(2k)$ )

```

APPENDIX (Continued)

```

# Plug in z

# n is the polynomial index

sum_total = mp.diff(lambda x: mp.pcf(n, a*x), z)

sum_total = sum_total/a

return sum_total


def parabola_vec(eta, x_all):

    # Calculate the vectors to plot the parabolas for a given setup

    x_final = []

    y_final = []

    for x in x_all:

        try:

            y_pos = sqrt((2*x + eta**2) * eta**2)

            y_neg = -sqrt((2*x + eta**2) * eta**2)

            x_final.append(x)

            x_final.append(x)

            y_final.append(y_pos)

            y_final.append(y_neg)

        except:

```

APPENDIX (Continued)

```

        continue

    data = {'x': x_final, 'y': y_final}

    df = pd.DataFrame(data)

    df = df.sort_values(by=['y'], axis=0, ascending=True)

    return df['x'].tolist(), df['y'].tolist()

def cyl2pc(rho, phi):
    # Convert from cylindrical coordinates (rho, phi) to parabolic cylinder
    # coordinates (eta, xi). Input rho must be in radians, not degrees

    eta = sqrt(rho * sin(phi) * tan(phi/2))

    if phi > pi:
        xi = - sqrt(rho*(1 + cos(phi)))
    else:
        xi = sqrt(rho * (1 + cos(phi)))

    pc_crd = [eta, xi]

    return pc_crd

def abc_calculate(n, Y_1, Y_2, eta_1, eta_2, g_plus, g_minus):

```


APPENDIX (Continued)

```

c_n = Y_2*((1j * pcdf_prime(n, eta_2, g_minus)) + (pcfd(n, eta_2 * g_minus)
↪ *pcdf_prime(-n-1, eta_2, g_plus) / pcfd(-n-1, eta_2 * g_plus))) *
↪ ((Y_2 * (pcdf_prime(-n-1, eta_2, g_plus) / pcfd(-n-1, eta_2 *
↪ g_plus)) * (pcfd(-n-1, eta_2 * g_plus) - (pcfd(-n-1, eta_1 * g_plus)
↪ * pcfd(n, eta_2 * g_minus) / pcfd(n, eta_1 * g_minus)))) - (1j * Y_1 *
↪ (pcfd(-n-1, eta_1 * g_plus) * pcdf_prime(n, eta_2, g_minus) /
↪ pcfd(n, eta_1 * g_minus)))) - (Y_1 * pcdf_prime(-n-1, eta_2,
↪ g_plus)))*(-1))

```

```

a_n = (1/pcfd(-n-1, eta_2*g_plus)) * c_n *(pcfd(-n-1, eta_2 * g_plus) -
↪ (pcfd(-n-1, eta_1 * g_plus) * pcfd(n, eta_2 * g_minus) / pcfd(n,
↪ eta_1 * g_minus)))) - (pcfd(n, eta_2 * g_minus)/pcfd(-n-1, eta_2 *
↪ g_plus))

```

```

b_n = -c_n * pcfd(-n-1, eta_1 * g_plus) / pcfd(n, eta_1 * g_minus)

```

```

return [a_n, b_n, c_n]

```

APPENDIX (Continued)

A.2 Calculating Script

The python script in this section calculates the field scattered by our PEC parabolic cylinder coated in an isorefractive sheath as a function of scattering angle ϕ . The code is written for python 3.6. The code is currently configured to calculate the fields according to Table I, with an angle of incidence of $\phi_0 = 135^\circ$. The results are saved to a file for plotting, which can be accomplished using the code presented in A.3.

```

### Calculate Sheath E Polarized Asymptotic

# Calculate the power scattered for the case of a plane wave in a parabolic
→ geometry scattering off an isorefractively sheathed PEC parabolic cylinder
→ in the far-field as a function of angle, here using the asymptotic limit.

from pcf_lib import *

from mpmath import sin, cot, factorial, pcfd, exp, fabs

import numpy as np

import pickle

from decimal import Decimal

from math import pi

# Constants

phi_0 = np.deg2rad(170)           # angle of incidence

eta_1 = 10                        # surface of the PEC

```

APPENDIX (Continued)

```

eta_2 = 12    # Surface of the IR cylinder

n_max = 51    # Number of iterations

phi_samples = 181

# Constants for angular analysis

phi = np.linspace(np.pi/2, 3*np.pi/2, phi_samples)

# Isorefractive Condition

c_light_speed = 3e8

wave_length_lambda = 3000

freq = (c_light_speed/wave_length_lambda)

print(freq)

k = 2*pi/wave_length_lambda # Wave number - highly should simplify
    ↪ calculations

print("k is {}".format(k))

omega = c_light_speed * (2*pi) / wave_length_lambda    # Angular frequency -
    ↪ here we're trying to lower the total value of the Y's

print("omega is {}".format(omega))

sqr_k_omega = (k/omega)**2

mu_1 = 1

```

APPENDIX (Continued)

```
epsilon_1 = sqr_k_omega/mu_1
```

```
mu_2 = pi * 4e-7
```

```
epsilon_2 = sqr_k_omega/mu_2
```

```
Y_1 = sqrt(epsilon_1/mu_1)
```

```
Z_1 = Y_1**-1
```

```
Y_2 = sqrt(epsilon_2/mu_2)
```

```
Z_2 = Y_2**-1
```

```
g_plus = exp(1j*pi/4) * sqrt(2*k)
```

```
g_minus = exp(-1j*pi/4) * sqrt(2*k)
```

```
# Create a filename for saving results for later processing
```

```
filename = 'sim-
```

```
→ ple_calculated_fields/sheath_E_asymptote/phi_{ }eta1_{:0.1e}_eta2_{:0.1e}_k_{:0.1e}_
```

```
→ eta_1, eta_2, k, n_max, omega, mu_1, mu_2)
```

```
filename = filename.replace('.', '_')
```

```
# calculate the Coefficients of expansion
```

```
a_n = np.zeros(n_max, dtype=complex)
```

APPENDIX (Continued)

```

c_n = np.zeros(n_max, dtype=complex)

b_n = np.zeros(n_max, dtype=complex)

print("Calculating Coefficients")

for n in range(0, n_max):

    # c_n - this is a long, cumbersome calculation

    a_n[n], b_n[n], c_n[n] = abc_calculate(n, Y_1, Y_2, eta_1, eta_2, g_plus,
        ↪ g_minus)

print("Coefficients Complete!")

# Create our parabolic cylinder coordinate system

Z = np.zeros((len(phi), n_max)) # Create an array of zeros

# Create empty arrays to hold the solutions of E and S

E_n = np.array(Z, dtype=complex)

S_n = np.array(Z, dtype=complex)

# Let's calculate the actual electric field as a function of phi in the
    ↪ asymptotic expansion. We are ignoring the

# contribution from constants in the final expression.

```

APPENDIX (Continued)

```

for n in range(0, n_max):

    print("E calculation n is {}".format(n))

    for i in range(0, phi.shape[0]):

        # print("i is {}".format(i))

        E_n[i, n] = (1/sin(phi_0/2)) * (((1j * cot(phi_0/2))**n)/factorial(n))
        ↪ * a_n[n] * (cot(phi[i]/2))**n / sin(phi[i]/2)

# Calculate the normalized power pattern of the sum of every element up to
↪ this point. i.e. S_n[0] is the power pattern for the first term n. S_n[10]
↪ is the sum of the first 11 terms. S_n[100] is the sum of the first 101
↪ terms, etc...

for n in range(0, n_max):

    print("S calculation n is {}".format(n))

    E_temp = E_n[:, 0:n+1]

    for i in range(0, phi.shape[0]):

        S_n[i, n] = fabs(E_temp[i, :].sum(axis=0))**2

# Save the variables for further analysis

with open(filename, 'wb') as f:

    pickle.dump([E_n, S_n, phi, eta_1, eta_2, k, omega, mu_1, mu_2, n_max,
    ↪ float(phi_0)], f)

```

APPENDIX (Continued)

```
print('save complete')
```

A.3 Plotting Script

The python script in this section plots the fields calculated in A.2 as a function of scattering angle ϕ . The code is written for python 3.6. The code loads the saved results from the calculation script, and saves the resulting plots for future reference.

```
### Plot sheath E angular ###

# Plot the scattered electric field from an isorefractive sheath as a
# function of scattering angle.

import matplotlib.pyplot as plt

import os

import pickle

import numpy as np

from math import pi

### Inputs ###

home_path = 'simple_calculated_fields/sheath_E_asymptote/'

plot_path = home_path + 'plots'
```

APPENDIX (Continued)

```

file_path_1 = home_path + 'phi_135_0_eta1_1_0e+01_eta2_1_2e+01_k_2_1e-
↪ 03_n_51_omega_6_3e+05_mu1_1_0e+00_mu2_1_3e-06'

print(file_path_1)

this_title = input('What would you like to call these plots?')

if not os.path.exists(plot_path):
    os.makedirs(plot_path)

### Load the saved calculations ###

print('load your file')

with open(file_path_1, 'rb') as f:

    [E_n, S_n, phi, eta_1, eta_2, k, omega, mu_1, mu_2, n_max, phi_0] =
    ↪ pickle.load(f)

##### Total Field #####

E_0 = E_n[:, 0]

E_1 = np.sum(E_n[:, 0:2], axis=1)

```


APPENDIX (Continued)

```

E_2 = np.sum(E_n[:, 0:3], axis=1)

E_3 = np.sum(E_n[:, 0:4], axis=1)

E_4 = np.sum(E_n[:, 0:5], axis=1)

E_5 = np.sum(E_n[:, 0:6], axis=1)

E_10 = np.sum(E_n[:, 0:11], axis=1)

E_20 = np.sum(E_n[:, 0:21], axis=1)

##### Phase Angle #####

E_0_angle = (np.angle(E_0) + (2* np.pi)) % (2*np.pi)
E_1_angle = (np.angle(E_1) + (2* np.pi)) % (2*np.pi)
E_2_angle = (np.angle(E_2) + (2* np.pi)) % (2*np.pi)
E_3_angle = (np.angle(E_3) + (2* np.pi)) % (2*np.pi)
E_4_angle = (np.angle(E_4) + (2* np.pi)) % (2*np.pi)
E_5_angle = (np.angle(E_5) + (2* np.pi)) % (2*np.pi)
E_10_angle = (np.angle(E_10) + (2* np.pi)) % (2*np.pi)
E_20_angle = (np.angle(E_20) + (2* np.pi)) % (2*np.pi)

print('plotting it')

### Labels for plots ###

```

APPENDIX (Continued)

```
label_1 = "n = 0"
```

```
label_2 = "n = 1"
```

```
label_3 = "n = 2"
```

```
label_4 = "n = 3"
```

```
label_5 = "n = 4"
```

```
label_6 = "n = 5"
```

```
label_7 = "n = 10"
```

```
label_8 = "n = 20"
```

```
##### Plot the total magnitude #####
```

```
super_title_3 = "Far-Field Scattering by an Isorefractive Parabolic Sheath \n
```

```
↪ " \
```

```
"|$\Psi_s (\phi)$|, $\phi_0$:
```

```
↪ {:.0f}$^\circ$".format(np.round(np.rad2deg(phi_0),0))
```

```
sum_title = "Sum Over $n$ Iterations"
```

```
fig3 = plt.figure()
```

```
fig3.set_size_inches(10, 10)
```

```
fig3.suptitle(super_title_3)
```

APPENDIX (Continued)

```
ax3 = fig3.add_subplot(111, polar=True)

ax3.set_thetamin(90)

ax3.set_thetamax(270)

ax3.set_theta_zero_location("E")


ax3.plot(phi, np.absolute(E_0), label=label_1, color='blue', linewidth=5,
→ linestyle= '-')

ax3.plot(phi, np.absolute(E_1), label=label_2, color='green', linewidth=4,
→ linestyle= ':')

ax3.plot(phi, np.absolute(E_2), label=label_3, color='red', linewidth=2,
→ linestyle= '-.')

ax3.plot(phi, np.absolute(E_3), label=label_4, color='black', linewidth=2,
→ linestyle= '--')

ax3.plot(phi, np.absolute(E_4), label=label_5, color='orange', linewidth=4,
→ linestyle= ':')

ax3.plot(phi, np.absolute(E_5), label=label_6, color='cyan', linewidth=1,
→ linestyle= '-')

ax3.plot(phi, np.absolute(E_10), label=label_7, color='gray', linewidth=2,
→ linestyle= '-')
```

APPENDIX (Continued)

```

ax3.plot(phi, np.absolute(E_20), label=label_8, color='black', linewidth=1,
→  linestyle= ':')

y_min, y_max = plt.ylim()

plt.arrow(phi_0, .8*y_max, 0, -.3*y_max, color='black', Linewidth=3,
→  head_width=0.05)

plt.text(phi_0-0.01, .85*y_max, r'$\phi_0 = $
→  {:.0f}$^\circ$'.format(np.round(np.rad2deg(phi_0),0)))

plt.xticks((pi/2, 3*pi/4, pi, 5*pi/4, 3*pi/2), ('$pi/2$', '$3pi/4$',
→  '$pi$', '$5pi/4$', '$3pi/2$'))

ax3.legend(bbox_to_anchor=(1.1, 0.8), title=sum_title)

##### Plot the phase angle #####

super_title_4 = "Far-Field Scattering by an Isorefractive Parabolic Sheath \n
→  " \

        "Phase Angle of $\Psi_s (\phi)$, $\phi_0$:
→  {:.0f}$^\circ$".format(np.round(np.rad2deg(phi_0),0))

fig4 = plt.figure()

fig4.set_size_inches(7, 7)

```

APPENDIX (Continued)

```

fig4.suptitle(super_title_4)

ax4 = fig4.add_subplot(111)

ax4.plot(phi, E_0_angle, label=label_1, color='blue', linewidth=5, linestyle=
↳ '-')

ax4.plot(phi, E_1_angle, label=label_2, color='green', linewidth=4, linestyle=
↳ ':')

ax4.plot(phi, E_2_angle, label=label_3, color='red', linewidth=2, linestyle=
↳ '-.')

ax4.plot(phi, E_3_angle, label=label_4, color='black', linewidth=2, linestyle=
↳ '--')

ax4.plot(phi, E_4_angle, label=label_5, color='orange', linewidth=4,
↳ linestyle= ':')

ax4.plot(phi, E_5_angle, label=label_6, color='cyan', linewidth=1, linestyle=
↳ '-')

ax4.plot(phi, E_10_angle, label=label_7, color='gray', linewidth=2, linestyle=
↳ '-')

ax4.plot(phi, E_20_angle, label=label_8, color='black', linewidth=1,
↳ linestyle= ':')

ax4.arrow(phi_0, 7*pi/4, 0, -pi/2, color='black', linestyle="-", Linewidth=3,
↳ head_width=.05)

```

APPENDIX (Continued)

```

ax4.set_xlim((pi/2, 3*pi/2))

ax4.set_ylim((0, 2*pi))

ax4.set_xlabel('Scattering Angle  $\phi$ ')

ax4.set_ylabel('Phase Angle of Scattered Field  $\Psi_s(\phi)$ ')

box = ax4.get_position()

ax4.set_position([box.x0, box.y0, box.width * 0.7, box.height])

ax4.legend(loc='center left', bbox_to_anchor=(1, 0.5), title=sum_title)

ax4.grid()

plt.xticks((pi/2, 3*pi/4, pi, 5*pi/4, 3*pi/2), (' $\pi/2$ ', ' $3\pi/4$ ',
    ↪ ' $\pi$ ', ' $5\pi/4$ ', ' $3\pi/2$ '))

plt.yticks((0, pi/2, pi, 3*pi/2, 2*pi), ('0', ' $\pi/2$ ', ' $\pi$ ', ' $3\pi/2$ ',
    ↪ ' $2\pi$ '))

y_min, y_max = plt.ylim()

plt.text(phi_0+.07, .75*y_max, r' $\phi_0 =$ 
    ↪  $\{:.0f\}^\circ$ '.format(np.round(np.rad2deg(phi_0),0)))

##### Plot and save the figure #####

plt.show()

fig3.savefig(plot_path + '/' + this_title + '_total.png')

```

APPENDIX (Continued)

```
fig4.savefig(plot_path + '/' + this_title + '_phase.png')  
  
print('Plot saved successfully!')
```

CITED LITERATURE

1. Bowman, J. J., Senior, T. B. A., and Uslenghi, P. L. E.: Electromagnetic and Acoustic Scattering by Simple Shapes. New York, Hemisphere Pub. Corp., 1987.
2. Uslenghi, P. L. E.: Exact scattering by isorefractive bodies. IEEE Transactions on Antennas and Propagation, 45(9):1382–1385, Sep. 1997.
3. Newman, E. H.: Plane wave scattering by a material coated parabolic cylinder. IEEE Transactions on Antennas and Propagation, 38(4):541–550, April 1990.
4. Askarpour, A. N. and Uslenghi, P. L. E.: Exact radiation from dipole antennas on oblate spheroids coated with isorefractive and anti-isorefractive layers. IEEE Transactions on Antennas and Propagation, 60(11):5476–5479, Nov 2012.
5. Uslenghi, P. L. E. and Zich, R. E.: Radiation and scattering from isorefractive bodies of revolution. IEEE Transactions on Antennas and Propagation, 46(11):1606–1611, Nov 1998.
6. D. Erricolo, F. Mioc, P. U.: Exact scattering by a ridge on a metal plane with isorefractive quadrants. In Digest of National Radio Science Meeting, page 141, Salt Lake City, Utah, July 2000.
7. Erricolo, D., Greenenwald, K. A., and Uslenghi, P.: Radiation, penetration and scattering for a slotted semielliptical channel filled with isorefractive material - II. Numerical results based on eigenfunction expansions. In Digest of the National Radio Science Meeting, page 44, Boulder, CO, USA, Jan. 2002.
8. Erricolo, D., Lockard, M. D., Butler, C. M., and Uslenghi, P. L. E.: Numerical analysis of penetration, radiation, and scattering for a 2D slotted semielliptical channel filled with isorefractive material. PIER, 53:69–89, 2005.
9. Erricolo, D., Lockard, M., Butler, C., and Uslenghi, P.: Comparison among currents on surfaces inside and near a semielliptical channel filled with isorefractive material that backs a slotted plane: currents computed by analytical formulas and by integral equation methods. In Proc. Intl. Conf. on Electromagnetics in Advanced Applications (ICEAA'03), pages 469–474, Torino, Italy, Sept 2003.

10. Erricolo, D., Lockard, M., Butler, C., and Uslenghi, P.: Currents on conducting surfaces of a semielliptical-channel-backed slotted screen in an isorefractive environment. IEEE Trans. Antennas Propag., 53(7):2350–2356, July 2005.
11. Berardi, C., Erricolo, D., and Uslenghi, P. L. E.: Exact dipole radiation for an oblate spheroidal cavity filled with isorefractive material and aperture-coupled to a half space. IEEE Trans. Antennas Propag., 52(9):2205–2213, Sept. 2004.
12. Erricolo, D. and Uslenghi, P. L. E.: Exact radiation and scattering for an elliptic metal cylinder at the interface between isorefractive half-spaces. IEEE Trans. Antennas Propag., 52(9):2214–2225, Sept. 2004.
13. Erricolo, D. and Uslenghi, P.: Exact Radiation for Dipoles on Metallic Spheroids at the Interface Between Isorefractive Half-Spaces. IEEE Trans. Antennas Propag., 53(12):3974–3981, Dec. 2005.
14. Erricolo, D. and Uslenghi, P.: Exact Analysis of a 2D Cavity-backed Slot in a Ground Plane Covered by an Isorefractive Lens. In 2005 IEEE AP-S International Symposium and USNC/URSI National Radio Science Meeting, Washington,D.C, July 3-8 2005.
15. Valentino, M. and Erricolo, D.: Exact two-dimensional scattering from a slot in a ground plane backed by a semielliptical cavity and covered with an isorefractive diaphragm. Radio Sci., 42(RS6S12), Nov 2006. doi:10.1029/2006RS003547.
16. Valentino, M. and Erricolo, D.: Exact radiation of a dipole in the presence of a circular aperture in a ground plane backed by a spheroidal cavity and covered with an isorefractive diaphragm. Radio Sci., 42, 2007. RS6S13, doi:10.1029/2006RS003548.
17. Khaledian, S., Negishi, T., and Erricolo, D.: Exact scattering for an elliptic metal cylinder at the interface between antiisorefractive half-spaces. In USNC-URSI National Radio Science Meeting, Boulder, CO, USA, Jan. 6-9 2016.
18. Ghurye, G. S., Negishi, T., and Erricolo, D.: Exact scattering for a metallic spheroid at the interface between anti-isorefractive half-spaces. In USNC-URSI National Radio Science Meeting, Boulder, CO, USA, Jan. 6-9 2016.
19. Uslenghi, P.: Radiation, penetration and scattering for a slotted semielliptical channel filled with isorefractive material - I. Exact solutions. In Digest of the National Radio Science Meeting, page 43, Boulder, Co, USA, Jan. 2002.

20. Uslenghi, P.: TE-TM decoupling for scattering from isorefractive cylinders of arbitrary shape. In Proceedings of the International Symposium on Electromagnetic Theory, pages 432–433, Thessaloniki, Greece, May 1998.
21. Uslenghi, P.: Exact geometrical optics solution for an isorefractive wedge structure. IEEE Trans. Antennas Propag., 48(2):335–336, Feb. 2000.
22. Uslenghi, P.: Special solutions for isorefractive wedge. In Proc. Intl. Conf. on Electromagnetics in Advanced Applications (ICEAA'01), pages 421–423, Torino, Italy, Sept. 2001.
23. Butler, C. and Lockard, M.: Penetration into and radiation from a slotted semielliptical channel filled with an isorefractive material. Integral equation formulation and solution. In Digest of the National Radio Science Meeting, page 45, Boulder, CO, USA, Jan. 2002.
24. Liang, J. and Uslenghi, P.: Exact scattering by isorefractive paraboloidal radomes. IEEE Trans. Antennas Propag., 55(6, 1):1546–1553, Jun 2007.
25. Uslenghi, P.: Exact penetration, radiation and scattering for a slotted semielliptical channel filled with isorefractive material. IEEE Trans. Antennas Propag., 52(6):1473–1480, June 2004.
26. Uslenghi, P.: Exact geometrical optics scattering from a tri-sector isorefractive wedge structure. IEEE Antennas Wirel. Propag. Lett., 3:94–95, 2004.
27. Uslenghi, P. L. E.: Exact geometrical optics scattering from a right-angle isorefractive wedge structure. IEEE Antennas and Wireless Propagation Letters, 3(1):127–128, Dec 2004.
28. Uslenghi, P.: Exact radiation from two axisymmetric structures containing isorefractive materials. In Proc. IEEE Antennas and Propagat. Intl. Symp., volume 4, page 2880, 1999.
29. Scharstein, R. and Davis, A.: Time-domain three-dimensional diffraction by the isorefractive wedge. IEEE Trans. Antennas Propag., 46(8):1148–1158, Aug. 1998.
30. Roy, S. and Uslenghi, P.: Exact scattering for axial incidence on an isorefractive paraboloid. IEEE Trans. Antennas Propag., 45(10):1563, Oct. 1997.

31. Daniele, V. and Uslenghi, P.: Closed-form solution for a line source at the edge of an isorefractive wedge. IEEE Trans. Antennas Propag., 47(4):764–765, April 1999.
32. Valentino, M.: Elliptic and Spheroidal Shapes with a Cavity, a Lens and Isorefractive Media: EM Analysis and Evaluation. Master’s thesis, University of Illinois at Chicago, USA, 2005.
33. Askarpour, A. N. and Uslenghi, P. L. E.: Exact radiation from dipole antennas on prolate spheroids coated with isorefractive and anti-isorefractive layers. IEEE Trans. Antennas Propag., 60(4):2129–2133, Apr. 2012.
34. Uslenghi, P.: Scattering by a half-plane at the interface between isorefractive media. IEEE Antennas Wirel. Propag. Lett., 12:1662–1664, 2013.
35. Uslenghi, P.: Radiation of a line source over a half-plane located at the interface between isorefractive media. IEEE Antennas Wirel. Propag. Lett., 15:356–357, 2016.
36. Moon, P. H. and Spencer, D. E.: Field theory handbook : including coordinate systems, differential equations, and their solutions. Berlin; New York, Springer-Verlag, 1988.
37. Stutzman, W. and Thiele, G.: Antenna Theory and Design. Antenna Theory and Design. Wiley, 2012.
38. Ivanov, V. I.: Diffraction of short plane waves on a parabolic cylinder. Zh. Vychisl. Mat. Mat. Fiz., 2(2):241 – 254, 1962.
39. Erdélyi, A., Magnus, W., Oberhettinger, F., and Tricomi, F. G.: Higher Transcendental Functions. Vol. II. New York-Toronto-London, McGraw-Hill Book Company, Inc., 1953.
40. Abramowitz, M.: Handbook of Mathematical Functions, With Formulas, Graphs, and Mathematical Tables,. New York, NY, USA, Dover Publications, Inc., 1974.
41. Rudin, W.: Principles of Mathematical Analysis. International series in pure and applied mathematics. McGraw-Hill, 1976.
42. Weisstein, E. W.: Gamma function. From MathWorld—A Wolfram Web Resource. Last visited on 9/26/2019.

43. *NIST Digital Library of Mathematical Functions*. <http://dlmf.nist.gov/>, Release 1.0.24 of 2019-09-15. F. W. J. Olver, A. B. Olde Daalhuis, D. W. Lozier, B. I. Schneider, R. F. Boisvert, C. W. Clark, B. R. Miller, B. V. Saunders, H. S. Cohl, and M. A. McClain, eds.

VITA

NAME	Patrick James Martin
EDUCATION	B.S., Political Science, Certificate, Middle East Studies, University of Wisconsin - Madison, WI, 2010
	M.S., Physics, University of Illinois at Chicago, IL, 2016
	M.S., Electrical and Computer Engineering, University of Illinois at Chicago, IL, 2019
TEACHING	Undergraduate Physics PHYS 100 PHYS 106 PHYS 142